endometrial gland [9], umbilical cord blood [10], placenta [11], and amniotic membrane [6] have a high CTE and a beneficial effect on cardiac function. Therefore, we hypothesized that mesenchymal cells obtained from younger populations might have a better effect on regeneration therapies. As angiotensin receptor blocker (ARB) was known to have the potential to play a role in the anti-aging effect, we postulated that ARB might improve the efficacy of BM-MSCs on cardiac stem cell therapy.

Stimulation of angiotensin receptors is known to be related to adipogenic transdifferentiation of human BM-MSCs [16]. In the brain ischemic reperfusion model, BM-MSC transplantation significantly reduced the brain infarction area via improvement of brain blood flow and reduction of oxidative stress [17]. The effect of BM-MSC transplantation was abolished by knocking out the angiotensin-II (AT) receptor type-II (AT2R). On the other hand, this effect was restored by pretreatment with ARB for BM-MSCs in the culture. These facts suggest that ARB and stimulation of AT receptor may play a significant role in causing the angiogenesic effect of BM-MSC transplantation. Therefore, in this study, we investigated the effect of ARB on CTE of human BM-MSCs in vitro and in vivo, and efficacy of BM-MSC transplantation on cardiac function in the myocardial infarction (MI) model in vivo.

Materials and Methods

BM-Derived MSCs

Yub623 (RIKEN Cell bank, Cell No. HMS0017, Tokyo, Japan) cells were used as BM-MSCs in this study. Yub623 is a fibroblast-like shaped human MSC (hMSC) derived from neonatal human BM from a finger of patients with polydactyly. Cells were cultured in high-glucose supplemented Dulbecco's modified Eagle's medium containing 10% human serum.

Cardiomyogenic Induction and Chemical Agents

The method of cardiomyogenic induction in vitro was described previously (Supporting Information Material and Method-1) [6, 8–11]. In short, enhanced green fluorescent protein (EGFP) labeled BM-MSCs were cocultured with murine cardiomyocytes. In this system, the incidence of cell fusion was approximately 0.3% and the evidence of cell fusion-independent cardiomyogenesis was extensively shown in the previous studies [6, 8–11, 18, 19]. BM-MSCs were preincubated with chemical agent-containing medium for 2 weeks before coculture and/or cultured with chemical agent-containing medium after coculture. In this study, we used 3 μmol/l of telmisartan (tel), candesartan (cnd), losartan (los), olmesartan (olm), and valsartan (val) as an AT receptor blocker (ARB), 3 μmol/l of PD123319 (pd) as a specific AT type-I blocker; enalaprilat (ena) and captopril (cap) as an angiotensin converting enzyme (ACE) inhibitor; 3 μmol/l of aliskiren (ali) as a direct rennin inhibitor; 1 μmol/l of AT; and 10 μmol/l of GW9662 (gw) as a peroxisome proliferators-activated receptor-γ (PPAR-γ) blocker. Evaluation of efficiency of cardiomyogenic transdifferentiation was described previously [6, 10, 11]. In short, cocultivated BM-MSCs were enzymatically isolated, a smear sample was made, and then immunocytochemistry using mouse monoclonal antibody against anticardiac troponin-I (Trop-I, #4T21 Hytest, Euro, Finland) antibody was performed (described later). Isolated cells (spherical shape), in which Trop-I colocalized with EGFP at the cytoplasm were considered as Trop-I/EGFP double positive cells. The CTE was defined as the incidence of Trop-I/EGFP double positive cells in EGFP-positive BM-MSCs. The incidence of cell fusion was not affected by ARB treatment (0.30% to 0.39%) in this study.

Immunocytochemistry and Immunohistochemistry

A laser confocal microscope (FV1000, Olympus, Tokyo, Japan) was used. As described previously [6, 8–11, 18, 19], samples were stained with Trop-I with mouse monoclonal antibody (sigma) and rabbit polyclonal anti-connexin 43 antibody (sigma) diluted 1:300 overnight at 4°C, then stained with TRITC-conjugated anti-mouse IgG antibody (Sigma) and Cy5-conjugated anti-rabbit IgG antibody (Chemicon) diluted 1:100, containing 4′-6-diamidino-2-phenylindole (Wako) at 1:300 for 30 minutes at 25–28°C.

Enzyme-Linked Immunosorbent Assay

Angiogenic humoral factors (angiogenin, angiotensin-2, epidermal growth factor [EGF], basic fibroblast growth factor, heparin-binding EGF-like growth factor, hepatocyte growth factor, phosphatidylinositol-glycan biosynthesis class F protein, and vascular endothelial growth factor) in culture medium supernatant (cultured with 10% serum-containing medium for 7 days) were measured by enzyme-linked immunosorbent assay [19]. The assay was performed with Quantibody Human Angiogenesis Array I kit (RayBiotec, Inc. GA) and was conducted according to manufacturer recommended protocol.

Gene Chip Analysis

Human genome-wide gene expression was examined with the Human Genome U133A Probe array (Affymetrix), which contains the oligonucleotide probe set for approximately 23,000 full-length genes and expressed sequence tags as described previously [11, 20].

Transplantation of ARB-Pretreated BM-MSCs in MI Model In Vivo

MI was induced in the open chests of anesthetized female F344 nude rats (Clea Japan, Inc., 6 weeks of age) as described previously [6, 9, 19]. Two weeks after MI, 1–2 $\times$ 10^6 of EGFP-labeled BM-MSCs were injected into the myocardium at the border zone of the MI. Two weeks after the first operation, rats with MI were randomized in a blind study of the following groups: the sham operated group (Sham), the (CNT), the CNT with plain BM-MSC transplanted group (BM), and the MI+candesartan-pretreated BM-MSC transplanted group (A-BM). After cellular transplantation, TCV-116 (stable form of candesartan; 0.5 mg/kg/day) was orally administered in some of the experiments (+A). Randomization occurred immediately before echocardiogram. Immediately before cell transplantation, two-dimensional and M-mode echocardiographic (8.5 MHz linear transducer; EnVisor C, Phillips Medical System, Andover, MA) images were obtained to assess left ventricular (LV) end-diastolic dimension and LV end-systolic dimension (LVESD) at the mid-papillary muscle level by a single blinded observer. Two weeks after the transplantation, a similar echocardiogram was performed again. LV percentage fractional shortening, thickness of anterior wall (AW), and thickness of posterior wall were calculated from five to six traces and averaged. LV pressure, brain natriuretic peptide (BNP), body weight, and heart weight (wet) were measured as described previously. Tissue samples were obtained by slicing along the short axis of the left ventricle, for every 1 mm of depth. After masson trichrom staining, the area of fibrosis was digitized from each slice, and then the percentage fibrosis volume in the LV myocardium was calculated as described previously [6, 19]. Immunohistochemical analysis was performed to observe CTE in vivo as described previously (Supporting Information Material and Method-2). Immunohistochemical analysis was performed using anti-rat CD34 antibody (1:200 R&D Systems; AF4117) to evaluate vascular density. Then, biotinylated goat immunoglobulins (Dako; E0466) were used as a second antibody, next, strept avidin biotin complex (ABC) complex/horseradish peroxidase (HRP) (Dako; K0377), and, finally, 3,3′-Diaminobenzidine substrate (Wako; K3183500) were used. The images were digitized and the percentage brown pixel area of the capillary vessels was counted in the peri-infarct normal zone (NZ) and the center of the MI

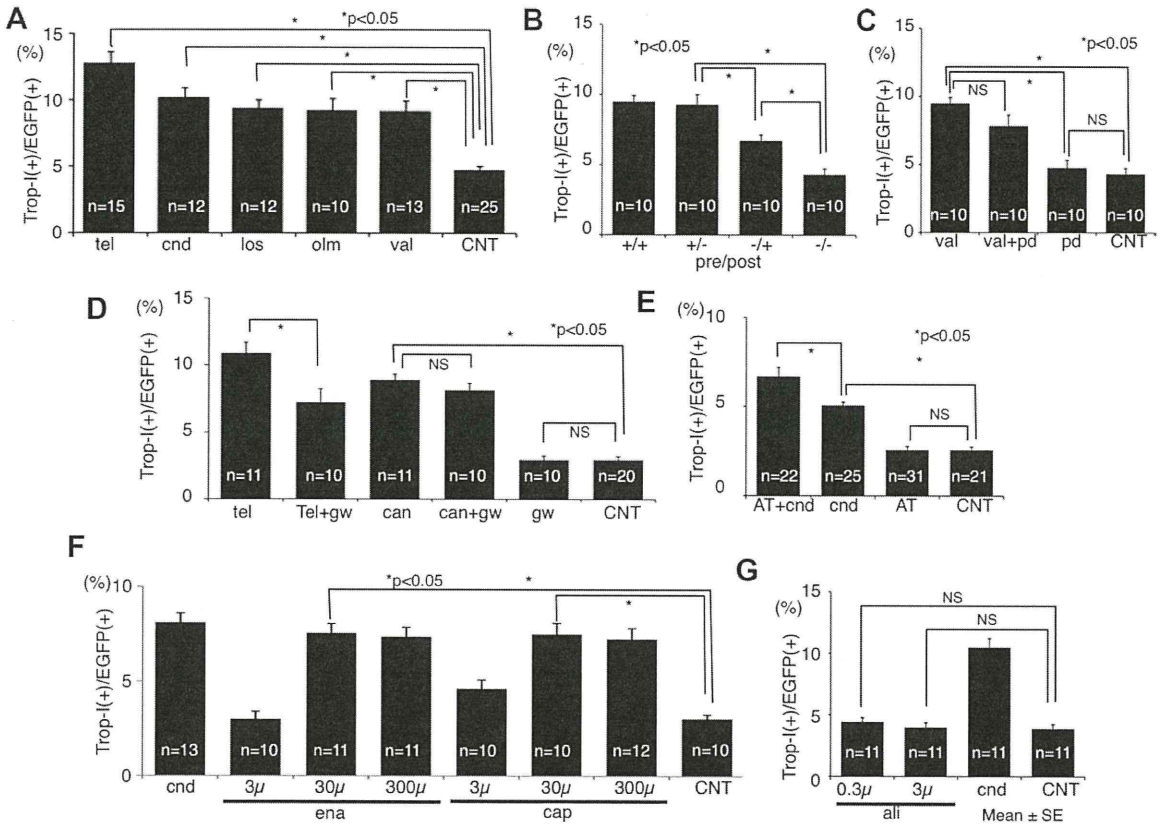

Figure 1. Improvement of cardiomyogenic transdifferentiation efficiency (CTE) of bone marrow-derived mesenchymal stem cells (BM-MSC) by blockade of renin-angiotensin system in vitro. The calculated rate of cardiac troponin-I positive cells in enhanced green fluorescent protein-positive cells are averaged and shown as CTE. **(A):** The effect of pretreatment with telmisartan (tel), candesartan (cnd), losartan (los), olmesartan (olm), and valsartan (val) on CTE of human BM-MSCs are shown. CNT denoted CTE of control MSCs. These ARBs increase CTE significantly. **(B):** Condition of pretreatment of val (before slash) and val treatment after induction (after slash) are shown in the bottom. Pretreatment of val significantly increased CTE and was essential for val-induced CTE increase. Val treatment after induction moderately increased CTE. **(C):** The effect of combination of val as a specific angiotensin-II (AT) receptor type-I (AT1R) blocker and PD123319 (pd) as a specific AT2R blocker to CTE is shown. The pd did not affect CTE. **(D):** The effect of GW9662 (gw) as a specific peroxisome proliferators-activated receptor-γ (PPAR-γ) blocker on tel-induced CTE increase and cnd-induced CTE increase are shown. The blockade of PPAR-γ partially blocked the tel-induced CTE increase and did not affect cnd-induced CTE increase. **(E):** The effect of additional application AT in the presence or in the absence of cnd is shown. AT alone did not affect CTE; however, AT significantly increased CTE in the presence of cnd. **(F):** Dose-response effect of pretreatment with enalaprilat (ena) and captoril (cap) as angiotensin converting enzyme inhibitors (ACEI). ACEI significantly improves CTE in a dose-dependent manner. **(G):** The effect of aliskiren (ali) as a renin inhibitor on CTE is shown. Ali did not affect CTE. *p<0.05. Abbreviations: ali, aliskiren; AT, angiotensin-II; cap, captoril; cnd, candesartan; CNT, control; EGFP, enhanced green fluorescent protein; ena, enalaprilat; gw, GW9662; los, losartan; olm, olmesartan; pd, PD123319; Tel, telmisartan; Trop-I, troponin-I; val, valsartan.

zone (MI) using a light microscope at 10× magnification. The areas in five high-power fields were calculated and averaged.

Statistical Analysis

All data are shown as mean value ± SE. The difference between mean values was determined with one-way analysis of variance (ANOVA) test or one-way repeated measures ANOVA test and Bonferroni post hoc test. Statistical significance was set at $p < .05$.

Results

Pretreatment with ARB Increased Efficiency of Cardiomyogenic Transdifferentiation Via AT2R

Administration of 3 μmol/l of popular ARBs (tel, can, los, olm, and val) did not cause any significant change in morphology of BM-MSCs (Supporting Information Fig. 1A, 1B), while improved CTE in vitro was observed (Fig. 1A and Supporting Information Fig. 1C–1P). In our pilot study, we tested dose-response effect of ARBs and confirmed that this effect was saturated at the concentration of 3 μmol/l (CTE at control, 0.03, 0.3, 3, and 30 μmol/l of cnd were 3.0 ± 0.3, 3.5 ± 0.2, 4.8 ± 0.3, 8.9 ± 0.4, and 8.1 ± 0.5%, respectively). Therefore, in this study, we selected 3 μmol/l as a default concentration of ARBs. To clarify the target of the ARBs, val was administrated only before the coculture or only after the coculture (Fig. 1B). Administration of val after the start of coculture (±) caused modest improvement of CTE; on the other hand, administration of val before the start of coculture (±) significantly increased CTE, suggesting that val modified the character of the BM-MSCs so as to be able to cause higher CTE. To determine whether the effect of the ARBs was mediated by AT receptor type-I (AT1R) or AT2R, we used val as AT1R specific blocker and pd as AT2R specific blocker (Fig. 1C). Administration of pd did not affect CTE, while val increased CTE significantly. Furthermore, CTE with both val and pd administered did not show an additional increase

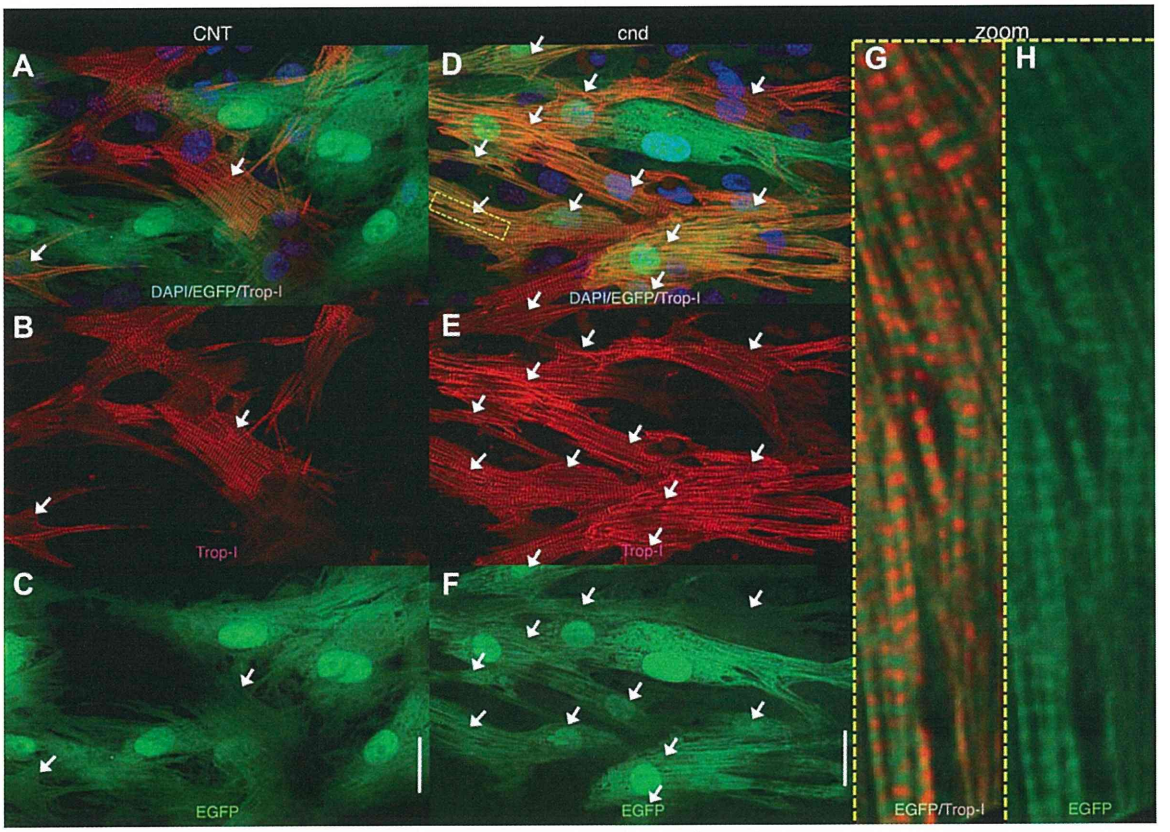

Figure 2. Confocal laser microscopic images of the immunocytochemical analysis of transdifferentiated cardiomyocytes. Confocal microscopic images of immunocytochemistry after cardiomyogenic induction using anti-cardiac troponin-I (red: Trop-I) revealed significant augmentation of enhanced green fluorescent protein (EGFP) (green)/Trop-I double positive cardiomyocytes (white arrow) by candesartan (cnd) (**D–F**) pretreatment, while EGFP/Trop-I double positive cells were rare in CNT (**A–C**). Area within the dotted yellow box is expanded and shown in (**G, H**). Clear striation staining pattern of Trop-I was observed in every EGFP-positive cell. The striating pattern of EGFP and Trop-I appeared in alternation, suggesting that the Trop-I was expressed in the EGFP-positive cells. Scale bar = 20 μm. Abbreviations: cnd, candesartan; CNT, control; DAPI, 4′-6-diamidino-2-phenylindole; EGFP, enhanced green fluorescent protein; Trop-I, troponin-I.

(rather, tended to show a statistically nonsignificant decrease). These data suggest that blockade of AT1R plays a pivotal role in ARB-dependent CTE increase. We have previously reported that PPAR-γ activator has an ability to increase CTE of BM-MSCs [19], and some of the ARBs, that is, tel, have a potential to activate the PPAR-γ. To clarify that the mechanism of ARB-induced CTE increase was mediated via PPAR-γ activation effect, we used gw as a specific blocker for PPAR-γ (Fig. 1D). The gw partially blocked tel-induced CTE increase; on the other hand, it did not block cnd-induced CTE increase. These data suggest that the effect of cnd on CTE was independent from PPAR-γ activation. In our previous study, the effect of pio was completely blocked by gw [19]; therefore, the gw-insensitive tel-induced CTE increase was caused by a PPAR-γ-independent mechanism. On the other hand, administration of AT did not affect CTE in the absence of ARB, while administration of AT significantly increased CTE in the presence of ARB (Fig. 1E). These data suggest both blockade of AT1R and stimulation of AT2R increase CTE. The increase in CTE was also observed by administration of ACE inhibitors ena or cap (Fig. 1F), suggesting the source of AT in this system is autocrine of angiotensin-I from BM-MSCs and local ACE activity. Furthermore, the effect was not blocked by the specific renin blocker, ali (Fig. 1G); therefore, angiotensinogen does not play a role as an AT source in this system, but a local angiotensin-generating system may play a role in this phenomenon.

The Effect of ARB-Treated BM-MSC Transplantation on Cardiac Function In Vivo

The BM-MSCs were transplanted into the hearts of nude rats with chronic MI, in vivo, and the effect on cardiac function was examined. Representative M-mode echocardiographic images at 2 weeks after transplantation are shown (Fig. 2A). In the CNT group, akinesis and thinning of AW are observed. There were no marked changes in the BM group, while in A-BM group, the motion of AW markedly improved. The same trend was also observed in the ARB orally administered group (+A group). The changes in echocardiographic parameters between the immediately before the transplantation group (post MI 2 weeks) and the 2 weeks after transplantation group (post MI 4 weeks) are compared (Fig. 3). Changes in LV ejection fraction (ΔLVEF) were decreased as a function of time, even 2 weeks after the MI, which may be due to LV remodeling. The transplantation of plain BM-MSCs (BM) did not have an effect on ΔLVEF; on the other hand, candesartan-pretreated BM-MSCs (A-BM) significantly improved ΔLVEF. The degree of improvement was marked when candesartan was orally administered (A-BM-A). Change in end-diastolic diameter of LV (ΔLVEDD) did not differ among the

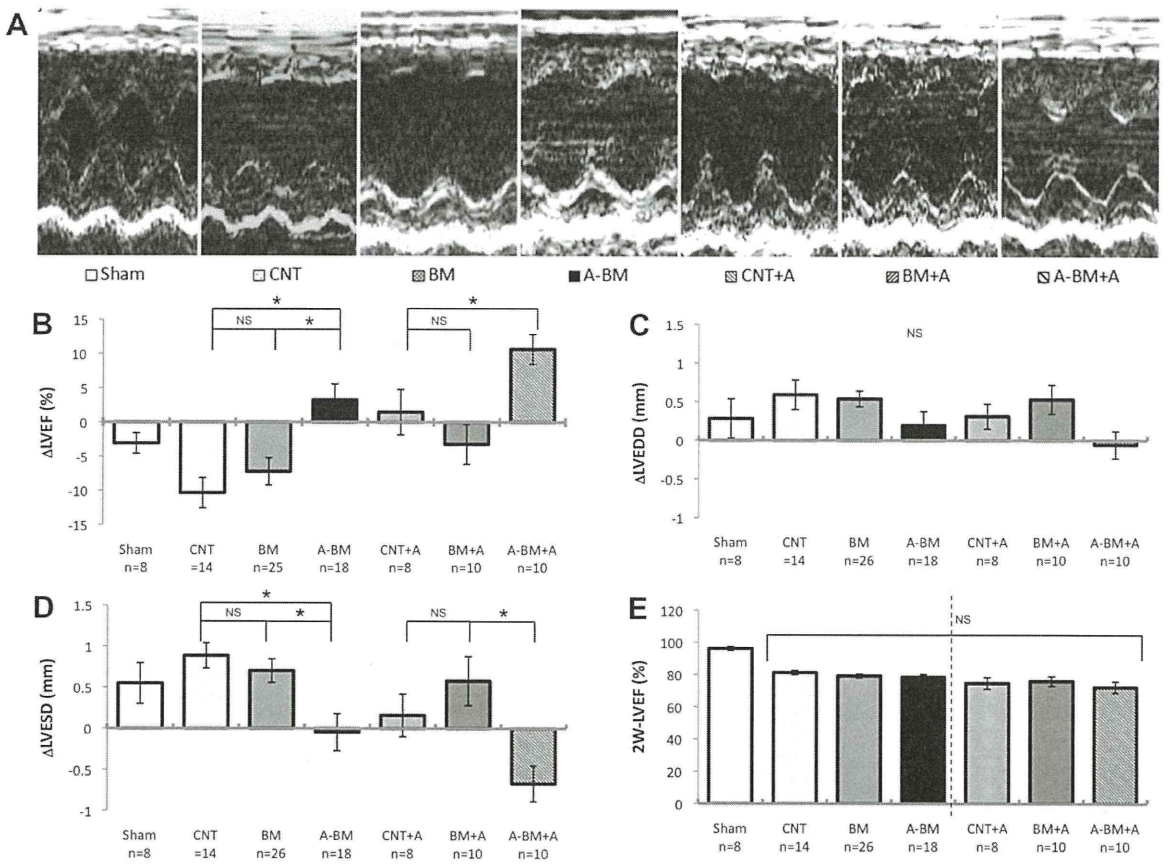

Figure 3. Effect of candesartan-pretreated bone marrow-derived mesenchymal stem cell (BM-MSC) transplantation and/or oral administration of candesartan on echocardiographic parameters in vivo. **(A):** Representative trace of M-mode echocardiogram from Sham-operated nude rats, control myocardial infarction (MI) (CNT), MI with BM-MSCs transplantation (BM), candesartan-pretreated BM (A-BM), and oral administration of candesartan after the transplantation (CNT+A, BM+A, A-BM+A) is shown. Changes in left ventricular ejection fraction (LVEF) from 2 to 4 weeks (**B**; ΔLVEF), LV end-diastolic dimension (**C**; ΔLVEDD), and LV end-systolic dimension (**D**; ΔLVESD) are averaged and shown. **(E):** Calculated LVEF from each group at 2 weeks after first operation are shown. There was no statistical significance; however, the degree of percentage EF tends to be worse in the oral administration series (right columns separated by dotted bar). Candesartan-pretreated BM significantly improved LVESD, consequently improved LVEF. *p<0.05. Abbreviations: BM, bone marrow; CNT, control; LVEDD, left ventricular end-diastolic dimension; LVEF, left ventricular ejection fraction; LVESD, left ventricular end-systolic dimension.

groups; on the other hand, change in LVESD (ΔLVESD) was significantly improved in A-BM group (vs. BM group) and A-BM+A group (vs. BM+A group), suggesting transplantation of candesartan-pretreated BM-MSCs significantly improved systolic function. Other echocardiographic parameter did not differ among the groups. There was no difference in the changes in body weight, serum BNP concentration, heart weight, LV systolic pressure, or LV end-diastolic pressure among the groups (Fig. 4). LV dP/dt was significantly improved by candesartan-pretreatment (A-BM vs. BM) with BM-MSCs; however, there was no additional effect of candesartan-pretreatment in the group of candesartan oral administration group (N.S. CNT-A vs. A-BM+A).

In this study, the beneficial effect was observed even in the ARB-pretreated BM-MSC transplantation group. The effect of ARB is known to cause an irreversible biological change in the cell, the "so-called" memory effect; therefore, such memory effect might affect cardiac function in vivo. To check this possibility, we cultured three groups of BM-MSCs: cells with candesartan for 2 weeks (ARB), cells without candesartan (CNT), and cells with candesartan for 1 week followed by 1 week without candesartan (1 week-ARB: washout for 1 week). The GeneChip analysis was performed among them, then the hierarchical clustering was used using the average distance method [20]. The gene expression pattern of 1 week-ARB was similar to CNT; therefore, the effect of ARB on BM-MSCs was reversible from the aspect of gene-chip analysis.

Incidence of Myocardial Transdifferentiation of ARB-Pretreated BM-MSCs In Vivo

To evaluate myocardial transdifferentiation of BM-MSCs in vivo, immunohistochemical analysis was performed. Antibodies against cardiac troponin-I (Trop-I) and connexin 43 were used. Confocal laser microscopic images could not detect EGFP-positive cardiomyocytes having clear striation staining pattern of Trop-I in the BM group. Sometimes enucleated EGFP-positive fragments of the cell at the center of the MI zone were observed, but taking the number of the injected EGFP-positive cells into account, the incidence seemed to be rare, as was reported previously [6, 19]. On the other hand, EGFP-positive and Trop-I double positive cells with clear striation staining pattern were observed at the marginal zone of the MI area in the candesartan-pretreated BM-MSC transplanted group (A-BM, Fig. 5F–5I). The oral

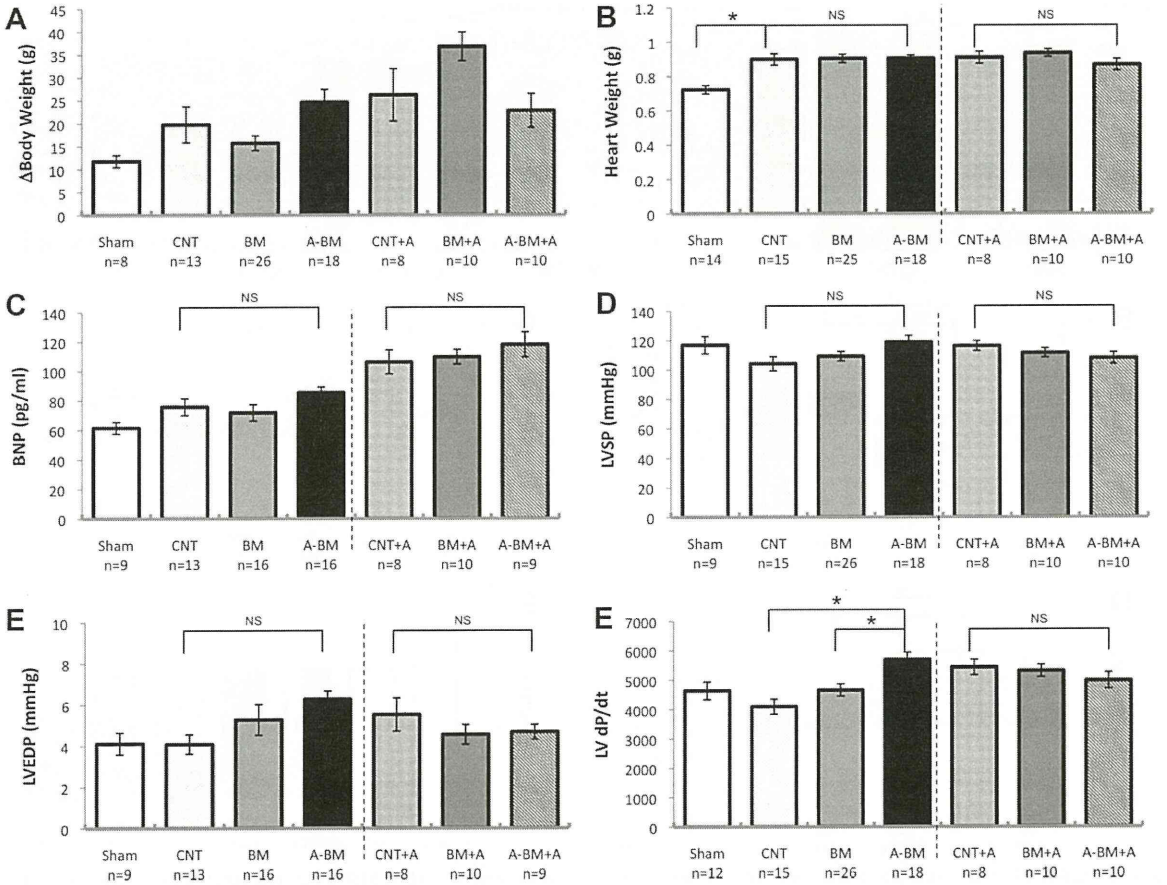

Figure 4. Effect of candesartan-pretreated bone marrow-derived mesenchymal stem cell (BM-MSC) transplantation and/or oral administration of candesartan on body weight, serum BNP concentration, and hemodynamic parameters. There was no difference in **(A)** changes in body weight, **(B)** heart weight, **(C)** BNP concentration, **(D)** left ventricular (LV) end-systolic pressure, or **(E)** end-diastolic pressure. **(D):** Effect of BM-MSCs on LV positive dP/dt is significantly improved by pretreatment with pioglitazone. **(F):** The LV dP/dt was significantly improved by transplantation of candesartan-pretreated BM-MSC (A-BM). *p<0.05. Abbreviations: BM, bone marrow; BNP, brain natriuretic peptide; CNT, control MI; LV, left ventricle; LVEDP, left ventricular end- pressure; LVSP, left ventricular systolic pressure.

administration of candesartan increased the incidence of survival of the EGFP/Trop-I double positive cells in vivo (A-BM+A, Fig. 5A–5E, 5J).

Genesis of Angiogenic Humoral Factors Derived from BM-MSCs by ARB

Angiogenic humoral factors were detected in the supernatant of the culture medium of BM-MSCs, suggesting that they are secreted from BM-MSCs, as reported previously [19]. However, the administration of 3 μmol/l of candesartan did not significantly affect the concentration of these angiogenic factors (Fig. 6). On the other hand, the angiogenic effect of candesartan-pretreated BM-MSCs was observed in vivo (Fig. 7A, 7B). In the peri-MI NZ, a CD34 positive area was not different among CNT, BM, and A-BM groups (without oral administration of candesartan). On the other hand, in the MI area, a CD34 positive area was significantly higher in A-BM group (vs. BM group). Oral administration of candesartan, significantly increased the CD34 area (CNT+A vs. CNT) in the peri-MI normal area and significantly increased it in the MI area. Masson trichrome staining and calculated MI volume at 2 weeks after transplantation (Fig. 7C, 7D) showed significant reduction of MI volume by pretreatment with candesartan of engrafted BM-MSCs (BM vs. A-BM) and the effect of pretreatment was not significantly augmented by the oral administration of candesartan.

Discussion

The Effect of Pretreatment with ARB in Human Neonatal BM-MSCs

The ARB did not affect the morphology of BM-MSCs and did not increase secretion of angiogenic humoral factors from BM-MSCs. The pretreatment with ARB significantly increased the CTE in vitro and in vivo. As pretreatment with ARB was essential for the effect on CTE, we concluded that the effect of ARB is not mediated by murine cultured myocardium, but directly affects BM-MSCs themselves, modifying the character of BM-MSCs. As the effect was not mediated by PD123319 as a selective AT2R blocker, the effect of ARB was mediated by the blockade of AT1R. In our previous article [19], activation of PPAR-γ significantly increased the CTE in BM-MSCs and the effect was completely blocked by GW9662, as a specific blocker of PPAR-γ receptor. The effect of telmisartan, which is known to have the strongest PPAR-γ activation activity among the ARBs, on CTE was partially blocked by GW9662, suggesting that the effect of ARBs is not mediated by PPAR-γ receptor activation activity. The

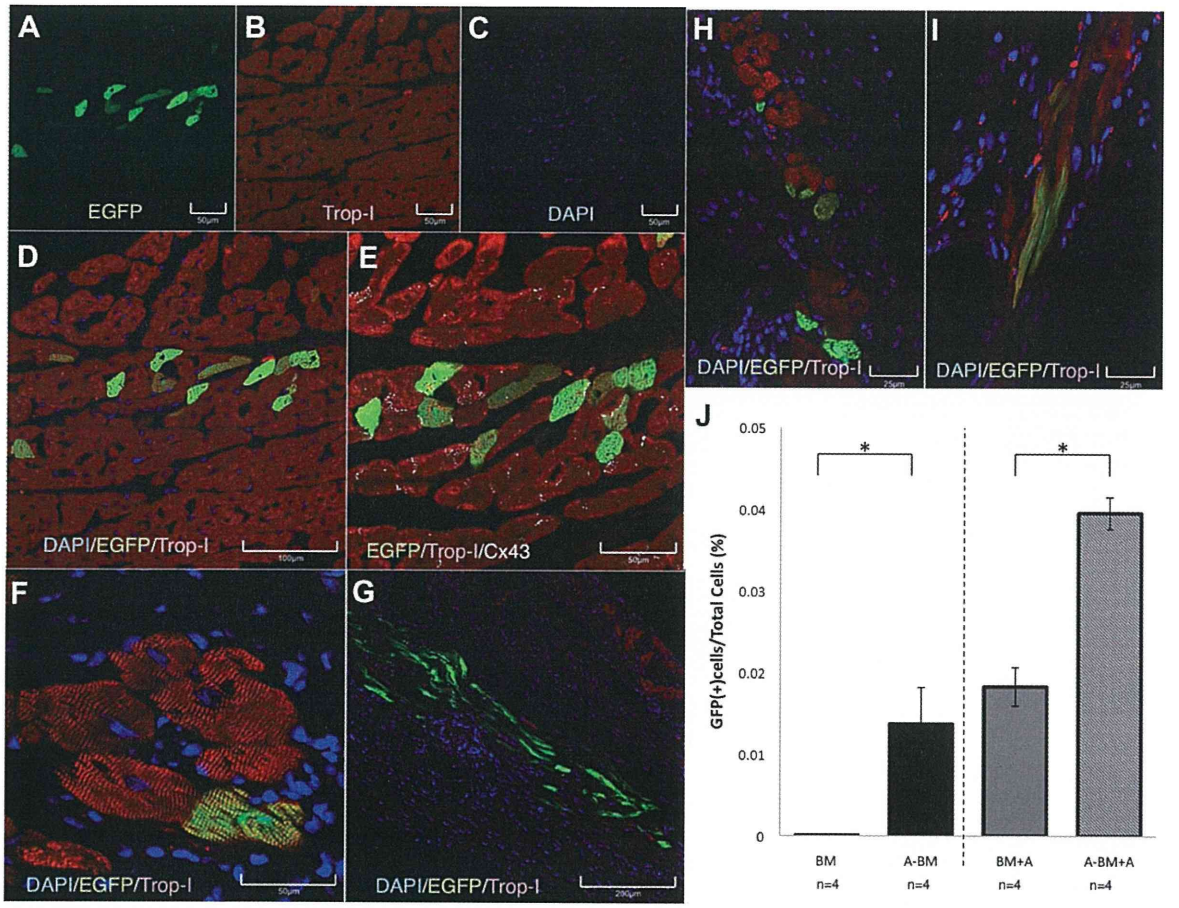

Figure 5. Both pretreatment and oral administration of candesartan significantly improved the incidence of survival of bone marrow-derived mesenchymal stem cell (BM-MSC)-derived cardiomyocytes in vivo. Confocal laser microscopic image of immunohistochemistry using anti-cardiac troponin-I antibody (red; Trop-I) is shown. **(A–C):** Lower magnification view for enhanced green fluorescent protein (EGFP) (green; **A**), Trop-I (**B**), and 4′-6-diamidino-2-phenylindole (Blue; **E**) is shown. After transplantation of candesartan-pretreated BM-MSCs in the presence of oral administration of candesartan (A-BM+A), EGFP-positive cells can be observed at the margin of the myocardial infarction (MI), but there were many EGFP/Trop-I double positive cardiomyocytes survived at the peri-MI zone (**A**). **(D):** Higher magnification view of merged image is shown. **(E):** The Trop-I positive cells are surrounded by dot-like staining of connexin 43 (white; Cx43). **(F):** Higher magnification view clearly shows striation staining pattern of Trop-I in the EGFP-positive cells. **(G):** At the center of MI zone (A-BM group), many EGFP-positive cells were enucleated and were negative for Trop-I. **(H, I):** However, there were some EGFP, Trop-I double positive rod-shaped cells at the center of MI zone. **(J):** The percentage of EGFP/Trop-I double positive cells in the injected EGFP-positive cells was averaged and is shown. By pretreatement with candesartan, the rate was significantly improved (A-BM vs. BM), and oral administration of candesartan additionally improved the incidence of EGFP/Trop-I double positive cells in vivo. Scale bars = 50 μm (**A–C, E, F**), = 100 μm (**D**), = 200 μm (**G**), and = 25 μm (**H, I**), respectively. *$p<0.05$. Abbreviations: BM, bone marrow; DAPI, 4′-6-diamidino-2-phenylindole; EGFP, enhanced green fluorescent protein; GFP, green fluorescent protein; Trop-I, troponin-I.

molecular mechanism of the effect of ARBs on CTE is still unclear. Further experiments should be done.

In the absence of valsartan as an AT1R selective blocker, administration of AT did not affect CTE; however, in the presence of valsartan, AT significantly increased CTE, suggesting that the relative stimulation of AT2R increased CTE. Furthermore, AT in culture medium seems to be generated by ACE activity in BM-MSCs, as the administration of ACE inhibitor to the BM-MSCs in culture significantly increased CTE in vitro. Furthermore, aliskiren did not affect the CTE; therefore, rennin and angiotensinogen did not play a role, but the angiotensin-I in the culture medium or autocrine from BM-MSCs must be a major source for AT.

Mechanism of Improving Systolic Function with ARB

Although EGFP-positive cardiomyocytes were observed in the candesartan-treated BM-MSC transplanted group, the number of them seems to be low for causing improvement in systolic function in vivo, as was seen in this study.

Concordant with the previous in vivo study [8] and clinical study [14], in the absence of BM-MSC transplantation, oral administration of candesartan suppressed the post-MI LV remodeling and progressive worsening of LVEF (CNT vs. CNT+A) at 2 weeks after MI. Furthermore, in this study, even in the absence of oral administration, the beneficial effect was observed in the candesartan-pretreated BM-MSC transplantation group. In this study, the effect of default BM-MSC transplantation was modest and there was no statistical significance from the control MI group. These data suggest that the ARBs modify the biology of BM-MSC, which play an important role in suppressing post-MI LV remodeling. This trend was observed in hemodynamic parameters and histological data. Pretreatment with candesartan significantly improved the efficacy of BM-MSC transplantation in augmentation of LV dP/dt and reduction in MI volume. Such

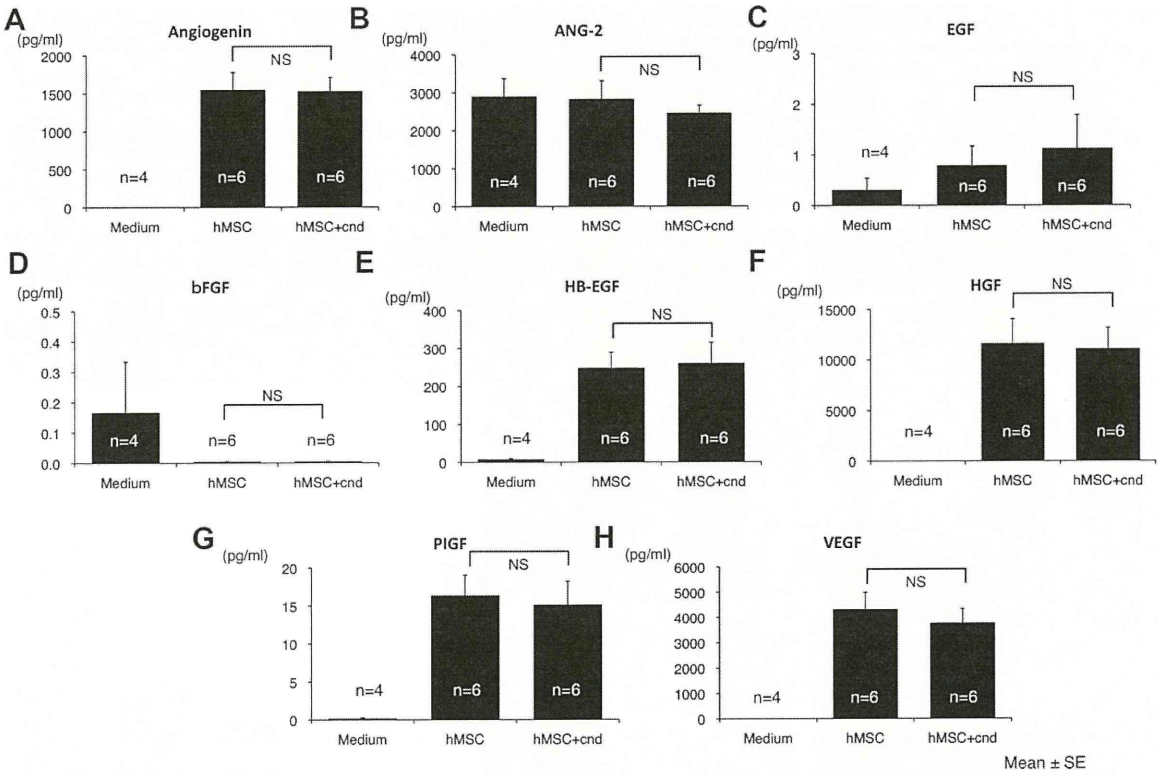

Figure 6. Secretion of angiogenic humoral factors from bone marrow-derived mesenchymal stem cells (BM-MSCs) into the culture medium supernatant and the effect of candesartan in vitro. Concentration of angiogenic humoral factors in **(A)** angiogenin, **(B)** angiotensin-2 (ANG-2), **(C)** epidermal growth factor (EGF), **(D)** basic fibroblast growth factor, **(E)** heparin-binding EGF-like growth factor, **(F)** hepatocyte growth factor, **(G)** phosphatidylinositol-glycan biosynthesis class F protein, and **(H)** vascular endothelial growth factor in culture medium was measured by enzyme-linked immunosorbent assay and averaged. Candesartan (cnd) treatment did not cause any significant change in angiogenic humoral factors secretion from BM-MSCs into the culture medium. Abbreviations: ANG-2, angiotensin-2; bFGF, basic fibroblast growth factor; cnd, candesartan; EGF, epidermal growth factor; HB-EGF, heparin-binding EGF-like growth factor; HGF, hepatocyte growth factor; hMSC, human mesenchymal stem cell; PIGF, phosphatidylinositol-glycan biosynthesis class F protein; VEGF, vascular endothelial growth factor.

cardioprotective effect of ARB-pretreated BM-MSCs may be due to augmentation of angiogenic effect and/or anti-apoptotic paracrine effect of BM-MSCs by pretreatment with ARB. The beneficial effect of ARB-pretreated BM-MSCs was also reported in the ischemia-reperfusion brain injury model [17], in which it was pointed out that both the stimulation of AT2R and blockade of AT1R have a significant effect on reducing brain damage in vivo and this data well correlated with our CTE data in vitro. In this study, the effect can be observed even by BM-MSC transplantation at 2 weeks after MI; therefore, the BM-MSC-induced angiogenesis might have suppressed ongoing post-MI LV remodeling. In this study, there was discrepancy between the angiogenic effect of ARB-pretreatment in BM-MSCs in vitro and in vivo. We speculated that additional angiogenic effect of BM-MSC transplantation by ARB-pretreatment might require graft-host interaction, that is, immunological reaction or inflammation in the host myocardium.

Cell Fusion-Independent Cardiomyogenic Transdifferentiation

Extensive evidence of cell fusion-independent cardiomyogenic transdifferentiation of human MSCs was presented in our previous study [6, 9–11, 19]. In this study, the incidence of cell fusion was approximately 1% and it was not affected by ARB pretreatment; therefore, the increase in EGFP-positive cardiomyocytes by ARB treatment was due to an increase in efficiency of cardiomyogenic transdifferentiation in vitro. Furthermore, there were no EGFP/Trop-I double positive rod shaped cardiomyocytes in the default BM-MSC transplanted group; on the other hand, the appearance of significant numbers of EGFP/Trop-I double positive cardiomyocytes was observed in ARB-pretreated BM-MSC transplanted group. This suggests an improvement of CTE of BM-MSCs in vivo by ARB pretreatment. Taking into account our previous study and our present in vitro experiment, we concluded that our observed EGFP/Trop-I double positive cells in vivo are caused by cardiomyogenic transdifferentiation.

Clinical Application

The efficacy of human BM-MSC transplantation had been modest [14, 15], and a new method for BM-MSC transplantation that will gain dramatic improvement in efficacy is expected. Genetic modification, that is, over-expression of the *AKT*-gene was reported to improve efficacy of BM-MSC transplantation in vivo [21]; however, use of such genetically modified cells raises a safety concern, that is, tumorgenecity. In comparison with the genetic modification, modification of BM-MSCs by ARBs, which are commonly used for heart failure patients, is a method that is ready to use for clinical patients.

In addition to the beneficial efficacy for cardiac function, this experimental model may also give us a clue to improving CTE in vivo, which is very essential for cardiac regenerative therapy. The precise mechanism for cardiomyogenic transdifferentiation of human BM-MSCs has been unclear. As the

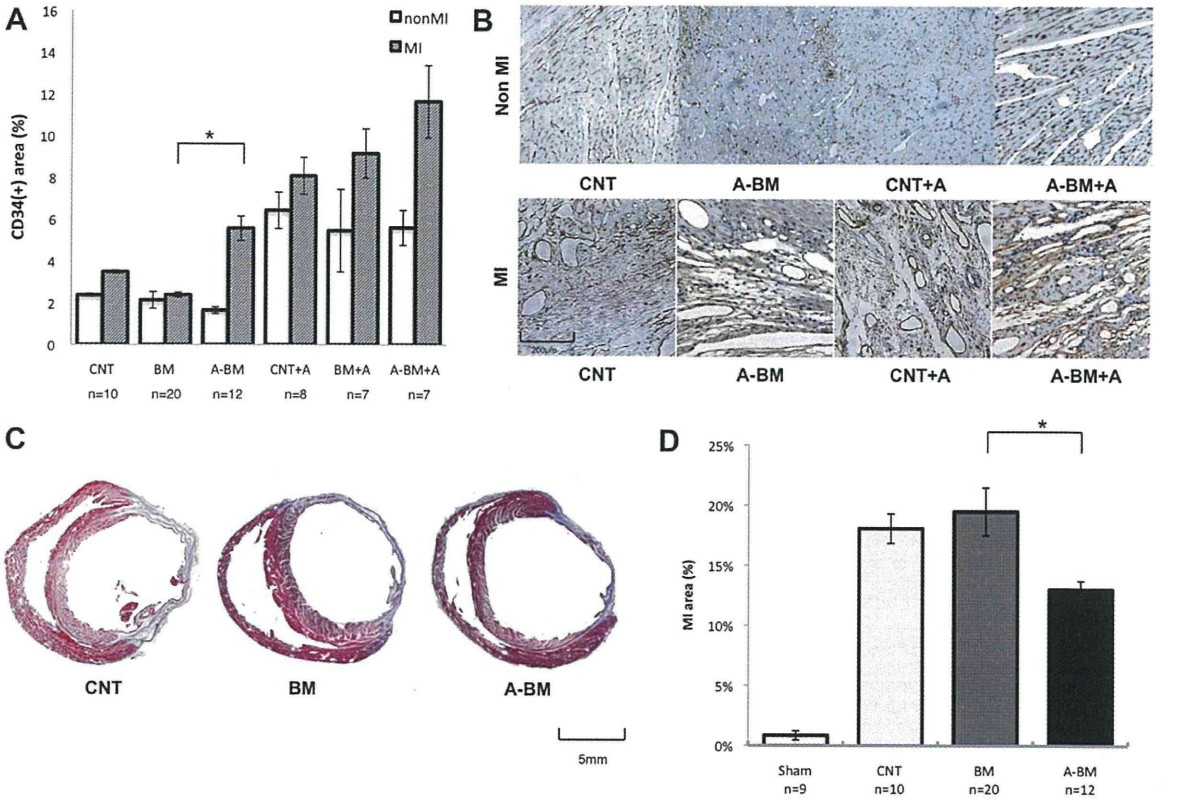

Figure 7. Effect of bone marrow-derived mesenchymal stem cell (BM-MSC) transplantation and/or treatment with candesartan on vessel density and infarction size in the heart in vivo. **(A):** The percentage of CD34 positive area in control myocardial infarction (MI) (CNT), MI with bone candesartan-pretreated BM-MSCs transplantation (BM), candesartan-pretreated BM (A-BM), and additional oral administration of candesartan after the transplantation (CNT+A, BM+A, A-BM+A) are calculated and averaged. **(B):** Representative microscopic image of immunohistochemistry using anti-CD34 antibody to detect vessels at center of MI zone and peri-MI normal zone (non-MI) are shown. Scale bar = 20 μm. Pretreatment with candesartan significantly increased vessel density at MI zone; on the other hand, oral administration of candesartan significantly increased vessel density at non-MI zone. **(C):** Representative masson-trichrom staining of the heart at the tendinous cord level of CNT, BM, and A-BM are shown. The digitized data were measured and calculated in **(D)**. By the candesartan-pretreatment, BM-MSC transplantation significantly decreased in percentage fibrosis volume. Scale bar = 5 mm. *p<0.05. Abbreviations: BM, bone marrow; CNT, control; MI, myocardial infarction.

incidence of cardiomyogenic transdifferentiation of human BM-MSCs is extremely rare, it has been impossible to statistically analyze the effect on CTE of various drugs or interventions in vivo. Therefore, there has been no systematic strategy for improvement of CTE of BM-MSCs until our previous article [6, 9–11, 19]. Our in vivo model of ARB-treated BM-MSCs is able to statistically analyze the effects of drugs on CTE, which is important for further improvement of CTE. In vitro, the pioglitazone's effect on CTE was independent from the effect of ARB; therefore, the additional administration of pioglitazone, as a PPAR-γ activator may be expected to improve CTE further. Further experiments should be done.

Study Limitation

In our previous study, we have used BM-MSCs obtained from a 41-year-old and a 90-year-old men. The CTE results were 1% and 0.3% in vitro [19], respectively. In this study, the CTE of default BM-MSCs from neonates was approximately 3%–5%. This data implies BM-MSCs obtained from younger generations that may have higher cardiomyogenic transdifferentiation ability. As ARB is known to have a potential for an anti-aging effect, the effect of ARB on BM-MSCs might increase the CTE by ARB's anti-aging effect on BM-MSCs. Further experiments should be done on this issue.

In vivo MI model was performed by two series (Sham, CNT, BM, A-BM series and CNT-A, BM-A, A-BM-A series) at different periods. As it was difficult to control the size of the MI at the coronary ligation, the size of the MI of later series are slightly larger (N.S.) than the former series. Therefore, we did not perform statistical analysis on some parameters between the series (separated by dotted line in the figures). The serum BNP level and the size of percentage MI volume are slightly larger in the later series. In this study, intra-individual difference values were compared with the values of the two series.

Conclusion

Pretreatment with angiotensin receptor blockers (ARBs) in culture activate human marrow-derived mesenchymal stem cells by angiotensin-II receptor type 1 blockade. ARBs-pretreated human marrow-derived msenchymal stem cells was significantly improved cardiomyogenic transdifferentiation efficiency in vitro and in vivo, and transplantation of the ARBs-pretreated cells significantly improved cardiac function and can be a promising cardiac stem cell source from which to expect cardiomyogenesis.

Acknowledgments

The research was partially supported by a grant from the Ministry of Education, Science and Culture, Japan. A part of this work was undertaken at the Keio Integrated Medical Research Center.

Disclosure of Potential Conflicts of Interest

The authors indicate no potential conflicts of interest.

References

1 Boheler KR, Czyz J, Tweedie D et al. Differentiation of pluripotent embryonic stem cells into cardiomyocytes. Circ Res 2002;91:189–201.
2 Makino S, Fukuda K, Miyoshi S et al. Cardiomyocytes can be generated from marrow stromal cells in vitro. J Clin Invest 1999;103:697–705.
3 Orlic D, Kajstura J, Chimenti S et al. Bone marrow cells regenerate infarcted myocardium. Nature 2001;410:701–705.
4 Tomita S, Li RK, Weisel RD et al. Autologous transplantation of bone marrow cells improves damaged heart function. Circulation 1999;100:II247–II256.
5 Asahara T, Murohara T, Sullivan A et al. Isolation of putative progenitor endothelial cells for angiogenesis. Science 1997;275:964–967.
6 Tsuji H, Miyoshi S, Ikegami Y et al. Xenografted human amniotic membrane-derived mesenchymal stem cells are immunologically tolerated and transdifferentiated into cardiomyocytes. Circ Res 2010;106:1613–1623.
7 Terai M, Uyama T, Sugiki T et al. Immortalization of human fetal cells: The life span of umbilical cord blood-derived cells can be prolonged without manipulating p16INK4a/RB braking pathway. Mol Biol Cell 2005;16:1491–1499.
8 Takeda Y, Mori T, Imabayashi H et al. Can the life span of human marrow stromal cells be prolonged by bmi-1, E6, E7, and/or telomerase without affecting cardiomyogenic differentiation? J Gene Med 2004;6:833–845.
9 Hida N, Nishiyama N, Miyoshi S et al. Novel cardiac precursor-like cells from human menstrual blood-derived mesenchymal cells. Stem Cells 2008;26:1695–1704.
10 Nishiyama N, Miyoshi S, Hida N et al. The significant cardiomyogenic potential of human umbilical cord blood-derived mesenchymal stem cells in vitro. Stem Cells 2007;25:2017–2024.
11 Okamoto K, Miyoshi S, Toyoda M et al. 'Working' cardiomyocytes exhibiting plateau action potentials from human placenta-derived extraembryonic mesodermal cells. Exp Cell Res 2007;313:2550–2562.
12 Grauss RW, Winter EM, van Tuyn J et al. Mesenchymal stem cells from ischemic heart disease patients improve left ventricular function after acute myocardial infarction. Am J Physiol Heart Circ Physiol 2007;293:H2438–H2447.
13 Hou M, Yang KM, Zhang H et al. Transplantation of mesenchymal stem cells from human bone marrow improves damaged heart function in rats. Int J Cardiol 2007;115:220–228.
14 Chen SL, Fang WW, Ye F et al. Effect on left ventricular function of intracoronary transplantation of autologous bone marrow mesenchymal stem cell in patients with acute myocardial infarction. Am J Cardiol 2004;94:92–95.
15 Hare JM, Traverse JH, Henry TD et al. A randomized, double-blind, placebo-controlled, dose-escalation study of intravenous adult human mesenchymal stem cells (prochymal) after acute myocardial infarction. J Am Coll Cardiol 2009;54:2277–2286.
16 Matsushita K, Wu Y, Okamoto Y et al. Local renin angiotensin expression regulates human mesenchymal stem cell differentiation to adipocytes. Hypertension 2006;48:1095–1102.
17 Iwanami J, Mogi M, Li JM et al. Deletion of angiotensin II type 2 receptor attenuates protective effects of bone marrow stromal cell treatment on ischemia-reperfusion brain injury in mice. Stroke 2008; 39:2554–2559.
18 Ikegami Y, Miyoshi S, Nishiyama N et al. Serum-independent cardiomyogenic transdifferentiation in human endometrium-derived mesenchymal cells. Artif Organs 2010;34:280–288.
19 Shinmura D, Togashi I, Miyoshi S et al. Pretreatment of human mesenchymal stem cells with pioglitazone improved efficiency of cardiomyogenic transdifferentiation and improved cardiac function. Stem Cells 2010 (in press).
20 Kami D, Shiojima I, Makino H et al. Gremlin enhances the determined path to cardiomyogenesis. PLoS One 2008;3:e2407.
21 Gnecchi M, He H, Liang O et al. Paracrine action accounts for marked protection of ischemic heart by Akt-modified mesenchymal stem cells. Nat Med 2005;11:367–368.

See www.StemCells.com for supporting information available online.

Lasers in Surgery and Medicine 43:984–990 (2011)

Myocardial Electrical Conduction Block Induced by Photosensitization Reaction in Exposed Porcine Hearts In Vivo

Arisa Ito, MSc,[1*] Shunichiro Miyoshi, MD,[2] Takehiro Kimura, MD,[2] Seiji Takatsuki, MD,[2] Kotaro Fukumoto, MD,[2] Keiichi Fukuda, MD, PhD,[2] and Tsunenori Arai, PhD[1]

[1]*School of Fundamental Science and Technology, Graduate School of Science and Technology, Keio University, 3-14-1, Hiyoshi, Kohoku-ku, Yokohama 223-8522, Japan*

[2]*Department of Cardiology, Keio University School of Medicine, 35 Shinanomachi, Shinjuku-ku, Tokyo 160-8582, Japan*

Background and Objective: This study proposes photosensitization reaction for non-thermal cardiac ablation in arrhythmia therapy. Acute and chronic phase experiments were conducted in exposed porcine hearts to demonstrate the photosensitization reaction-induced myocardial electrical conduction block *in vivo*.

Study Design/Materials and Methods: The porcine left atrial appendage was exposed under an open-chest procedure. Then, a water-soluble chlorin photosensitizer, NPe6, was injected into the pigs intravenously at 5 or 10 mg/kg. About 15 or 30 minutes after the injection, a 663-nm continuous-wave diode laser was irradiated on the surface of the atrial appendage through a silica optical fiber. The laser energy was delivered to the tissue point by point at an energy density of 50–208 J/cm^2.

Results: Acute and chronic tissue damages as a result of the photosensitization reaction were determined by electrophysiology and histology, respectively. The change in the myocardial conduction time between two electrodes was measured immediately after the completion of the 35-mm irradiation line between the electrodes. The conduction delay of 35.5 milliseconds might be due to the change in the conduction pathway induced by transmural acute conduction block with the photosensitization reaction. The tissue temperature increase in the irradiated area was approximately 12.8°C. Azan-staining revealed about 1-mm transmural fibrosis of the atrial appendage at 2 weeks after the irradiation (50 J/cm^2).

Conclusions: The results suggest that the photosensitization reaction might induce acute and chronic myocardial electrical conduction block. Cardiac ablation with the photosensitization reaction might be a non-temperature-mediated methodology for arrhythmia therapy. Lasers Surg. Med. 43:984–990, 2011.

Key words: arrhythmia; atrial fibrillation; cardiac ablation; NPe6; photodynamic therapy; photosensitizer

INTRODUCTION

The most common curative therapy for atrial tachyarrhythmia is radiofrequency catheter ablation to isolate arrhythmogenic foci [1–3]. The resistive heating of myocardium with radiofrequency energy induces thermal tissue injury in the pathway of ectopic beat conduction, resulting in myocardial electrical conduction block. However, there are several limitations of radiofrequency ablation including thermal complications (total incidence rate, 4–6%), such as thromboembolism and cardiac tamponade [4–6]. Alternative energy sources for cardiac ablation have been developed such as laser ablation, in which the laser energy is absorbed by the myocardium, resulting in temperature rise of tissue [7–9]. However, the laser ablation might face the same problem of the thermal complications as radiofrequency ablation. In spite of the relatively low incident rate of the thermal complications appeared in these thermal ablation therapies, totally beneficial methodologies are required compared to conservative treatment with medication.

We proposed the use of non-temperature-mediated cytotoxic process with photosensitization reaction to create a myocardial electrical conduction block. In clinical practice, photosensitization reaction is applied to a non-invasive cancer therapy known as photodynamic therapy (PDT) using photosensitizer specific accumulation to tumor tissue [10,11]. The photochemical interactions between photons, photosensitizer, and oxygen result in the generation of reactive oxygen species, mainly singlet molecular oxygen [12,13], which induce oxidative damage of biological molecules, resulting in apoptotic or necrotic cell death [14,15]. Since there is no photosensitizer specific accumulation in normal myocardium, particularly short drug–light intervals (approximately one-order shorter than the conventional interval) can be used in the application of photosensitization reaction for myocardial tissue.

Contract grant sponsor: The Japan Science and Technology Agency (Supporting Program for Creating University Ventures); Contract grant number: 1904; Contract grant sponsor: The Japan Society for the Promotion of Science (Research Fellowships for Young Scientists); Contract grant number: 3455.
*Corresponding to: Arisa Ito, MSc, 3-14-1, Hiyoshi, Kohoku-ku, Yokohama 223-8522, Japan. E-mail: arisa@a3.keio.jp
Accepted 19 September 2011
Published online in Wiley Online Library (wileyonlinelibrary.com).
DOI 10.1002/lsm.21136

The aim of this study was to demonstrate the feasibility of the application of photosensitization reaction for non-thermal cardiac ablation. Myocardial electrical conduction block caused by the photosensitization reaction with a water-soluble chlorin photosensitizer was examined electrophysiologically in an acute phase study and histopathologically in a chronic phase study with surgically exposed porcine hearts.

MATERIALS AND METHODS

Animal Preparation

The animal study was conducted with the approval of the Animal Care Committee in Keio University, Japan. LW female pigs weighing about 15 kg (1.5–2 months in age) for the acute phase study and about 24 kg (2–2.5 months in age) for the chronic phase study were sedated by injecting ketamine (2 mg/kg) and xylazine (2 mg/kg) intramuscularly, followed by mask-induced anesthesia with 5% isoflurane and pure O_2 at 1.5–2.0 L/minute. After tracheal intubation, general anesthesia was maintained by inducing inhalation of 2.5% isoflurane and pure O_2 at the same flow rate. The left cervical vein was cannulated for blood sampling. Standard limb-lead II electrocardiogram, heart rate, body temperature, and oxygen saturation by pulse oximetry were monitored continuously throughout the procedure.

Photosensitizer and Laser Light Source for In Vivo Study

A water-soluble chlorin photosensitizer, NPe6 (mono-L-aspartyl chlorin-e6), also known as talaporfin sodium, was used. NPe6 is approved in Japan as Laserphyrin® (Meiji Seika Kaisha, Ltd, Tokyo, Japan) for the treatment of early stage bronchopulmonary cancer [16]. This photosensitizer has a molecular weight of 799.69 and a significant absorption peak in the Q band at 664 nm [16–18]. NPe6 has a strong molar absorption coefficient of $4.0 \times 10^4\ M^{-1}\ cm^{-1}$ and a high quantum yield of singlet oxygen generation of 0.77 with the absorption peak in the Q band [18]. A 663-nm red diode laser was employed as a light source to excite NPe6 at the Q band. The laser light was delivered through a silica optical fiber with a core diameter of 1,200 μm.

Optical Characteristics of Porcine Myocardium

The optical properties of porcine myocardium were obtained using Kubelka–Munk two-flux theory, in which the scattering and absorption coefficients can be directly expressed in terms of the measured reflectance, transmittance, and thickness of the tissue sample [19]. Extracted porcine ventricular myocardium was cut in approximately 1-mm thick slices and placed between 0.2-mm-thick glass slides. The diffused transmittance and reflectance of the tissue samples were measured at 663 nm by a spectrophotometer (UV-3600; Shimadzu Co., Kyoto, Japan), equipped with an integrating sphere. The Kubelka–Munk coefficients A_{KM} and S_{KM} are related to transport coefficients using the following relations [20]:

$$A_{KM} = 2\mu_a, \quad S_{KM} = \frac{1}{4}(3\mu_s' - \mu_a) \tag{1}$$

The absorption coefficient, μ_a, and reduced scattering coefficient, μ_s', of the porcine myocardium were calculated with the measured diffused reflectance and transmittance.

Photosensitizer Concentration in Plasma

The NPe6 concentration in plasma during the procedure was measured to obtain the decay curve of the plasma concentration with time. The photosensitizer concentration in plasma might have a proportional relation to that in tissue; NPe6 concentration in heart is reported to be about one-sixth of that in plasma [21]. Porcine blood samples were collected in evacuated tubes containing ethylenediamine tetra-acetic acid (EDTA) 5–60 minutes after the photosensitizer injection. The blood samples were centrifuged at 3,000 rpm for 10 minutes at 4°C. The optical absorption spectra of NPe6 in the plasma were measured in the wavelength range of 350–710 nm by the spectrophotometer. The obtained absorption peak area of the Q band was determined using the baseline method and converted into the NPe6 concentration by comparison with a calibration curve constructed previously using known photosensitizer concentrations.

Electrophysiological Study in the Acute Phase

To demonstrate the acute and transmural electrical conduction block with the photosensitization reaction, we designed an electrophysiological study using porcine atrial appendage. The porcine chest was surgically opened, and the left atrial appendage (1–3 mm thickness) was exposed through an incision in the lateral chest wall. With the heart beating, two plunge electrodes (electrodes A and B) were inserted onto the atrial appendage. Electrode A was used for electrical stimulation of the myocardium with stimulation conditions of 6.3 milliseconds pulse width, 3.0 Hz frequency, and 1.5 V amplitude. Electrode B was used to measure the propagated activation signal. The measured electrical signals were amplified by Bio Amplifier (PowerLab, ADInstruments, Hastings, UK) and recorded by a computer with a data acquisition program, Chart 4 (ADInstruments). NPe6 dissolved in physiological saline was injected intravenously at 10 mg/kg into the pigs (around 15 kg, $n = 2$). The laser irradiation via the optical fiber started 30 minutes after the injection. The optical fiber was not in direct contact with the myocardial surface; instead, it was fixed by hand using a spacer to keep a constant distance of about 18 mm between the fiber tip and myocardial surface. The red laser light beam, with a spot size of 7 mm at a power density of 5.2 W/cm^2 and a total energy density of 208 J/cm^2, was irradiated point by point to make about 35-mm irradiation line between the two electrodes so that the adjacent irradiated areas overlapped by about 30%. The conduction time from electrode A to B was measured immediately (within 1 minute) after each irradiation to assess the acute

myocardial electrical conduction block by the photosensitization reaction. If the transmural conduction block was obtained during the procedure as in the case with radiofrequency ablation, the conduction time might be prolonged depending on the irradiation length to wrap around the transmural conduction block line.

Histopathological Study in the Chronic Phase

The porcine chest was surgically opened, and the left atrial appendage was exposed as described before. NPe6, dissolved in physiological saline at 5 mg/kg, was injected intravenously into pigs weighing about 24 kg ($n = 2$). Fifteen minutes after the injection, the red laser light beam was irradiated through the optical fiber on the surface of the atrial appendage as described previously with a spot size of 3 mm, power density of 3.5 W/cm^2, and total energy density of 50 or 100 J/cm^2. During the irradiation, the temperature change on the tissue surface was measured with an infrared thermo-camera (Avio TVS-500; Nippon Avionics, Ltd, Tokyo, Japan). Two weeks after the procedure, the pigs were euthanized, and their hearts were extracted and subsequently fixed in 10% formalin. The fixed heart samples were sectioned, and the cross-sectional slices at the irradiated sites were used to determine the area affected by the photosensitization reaction. The irradiated site was identified by the anatomical features of the appendage. The tissue specimens were stained with standard staining for histological examination; hematoxylin and eosin (HE) to examine the extent of viable or nonviable cells and changes in cellular and nuclear morphology, or Azan to differentiate between the normal and affected areas replaced by fibrotic (scar) tissue.

RESULTS

Optical Properties of the Porcine Myocardium at 663 nm

The absorption coefficient (μ_a), reduced scattering coefficient (μ_s'), effective attenuation coefficient (μ_{eff}), and optical penetration depth (δ) of the porcine ventricular myocardium at 663 nm were obtained by Equation (1). μ_{eff} and δ were obtained from the following equation: $\mu_{eff} = \delta^{-1} = \sqrt{3\mu_a(\mu_a + \mu_s')}$. The obtained parameters of the porcine myocardium were as follows: $\mu_a = 0.35\,mm^{-1}$, $\mu_s' = 0.68\,mm^{-1}$, $\mu_{eff} = 1.0\,mm^{-1}$, and $\delta = 0.96\,mm^{-1}$. The obtained absorption and scattering coefficients at 663 nm were within the range of previously reported data: $0.1 < \mu_a < 0.6\ mm^{-1}$, $0.6 < \mu_s' < 1.4\ mm^{-1}$ in the wavelength range of 600–700 nm [22,23].

Decay of NPe6 Concentration in Porcine Plasma

The NPe6 concentration in plasma between 5 minutes and 1 hour after the administration of 5 or 10 mg/kg NPe6 to the pigs ($n = 2$) during the procedure was measured. The plasma concentration of NPe6 decreased with time, exhibiting kinetics similar to previously reported data [24]. Similar to that reported in humans, the observed decay curve of plasma concentration with time could be divided in two phases [17]: the measured elimination half-life was about 7 minutes in the initial rapid exponential decline (the first phase) and about 77 minutes in the subsequent slower exponential decline (the second phase). In this study, the drug–light interval was determined to be 15–30 minutes, during which the NPe6 concentration in plasma was about 10 μg/ml, decreasing relatively gently in the second exponential decline phase. Our preliminary studies demonstrated the photosensitization reaction-induced electrical conduction block with a plasma concentration of 8 μg/ml in extracted rat hearts [25].

Acute Electrical Conduction Block With the Photosensitization Reaction

To demonstrate the acute myocardial electrical conduction block as a result of the photosensitization reaction, the conduction time of the electrical signal from electrode A to B after each irradiation was assessed using the exposed porcine left atrial appendage *in vivo* from the acute phase study. Figure 1 shows a macroscopic photograph of the left atrial appendage extracted immediately after the procedure, indicating the electrode arrangements and irradiated site. Although there was uneven coloration on the tissue surface of the atrial appendage due to variations in tissue thickness, we found no obvious evidence of acute thermal coagulation or edema formation. Figure 2 shows the electrical potential waveforms at the measuring electrode B immediately after each irradiation. The conduction time of the electrical signal generated at the

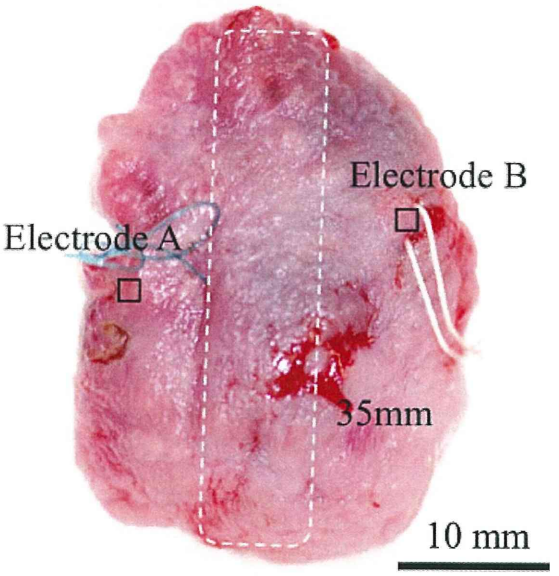

Fig. 1. A macroscopic photograph of a left atrial appendage extracted after the procedure. The extracted atrial appendage was washed with biological saline to remove blood. The area enclosed within the white dotted line shows the irradiated area. The length of the irradiated area is about 35 mm. The open squares indicate the sites of the stimulation and measurement electrodes in the myocardial tissue.

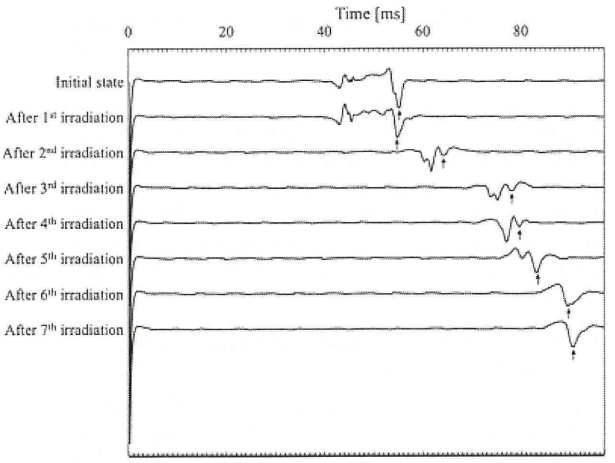

Fig. 2. The electrical potential signal recorded at electrode B in the initial state and after each irradiation. A shift in the electrical waveform indicates a conduction delay at electrode B as result of the photosensitization reaction. The black arrows indicate the time used to calculate the conduction time from stimulation to measurement at electrode B after each irradiation.

stimulated site and propagating to electrode B (t_{A-B}) was prolonged after each irradiation, indicating that the electrical response of the myocardium was obtained immediately (within 1 minute) after irradiation. The obtained values of t_{A-B} were 55.2 milliseconds at the initial state and 90.7 milliseconds after the sequence of the irradiations; a conduction delay of 35.5 milliseconds from the initial state was recorded.

Chronic Electrical Conduction Block as a Result of the Photosensitization Reaction

To demonstrate the permanent myocardial electrical conduction block as a result of the photosensitization reaction, chronic histopathological observations of the porcine left atrial appendage were examined *in vivo*. Figure 3 shows a macroscopic photograph of an extracted left atrial appendage fixed in formalin 2 weeks after the procedure. There were no obvious changes in tissue color on the surface of the irradiated area. Furthermore, there was no evidence of thermal damage in the irradiated area, which would be characterized by hemorrhage and edema surrounding coagulation necrosis. The measured temperature increase on the surface of the irradiated area during the irradiation was about 12.8°C. Figure 4 is a microscopic image of Azan- and HE-stained specimens at total energy densities of 50 J/cm^2, 2 weeks after the procedure. We found that the areas affected by the photosensitization reaction were demarcated and replaced transmurally with fibrosis tissue in the Azan-stained specimens (Fig. 4a). Neither myocardial wall rupture nor endocardial thrombi were observed. The maximum depths affected by the photosensitization reaction were >1.0 mm at a total energy density of 50 J/cm^2 and >1.3 mm at 100 J/cm^2.

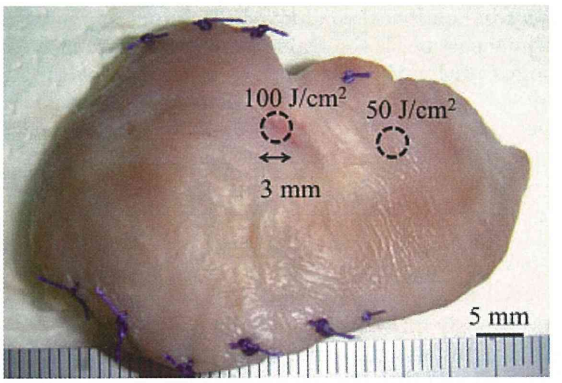

Fig. 3. A macroscopic photograph of a left atrial appendage fixed in formalin 2 weeks after the procedure. The dotted open circles indicate the irradiated sites.

Since the tissue thickness of the atrial appendage was around 1 mm in the irradiated area, the affected depth might exceed 1 mm under these irradiation conditions. There was almost no shrinkage in the affected area compared with the normal area, so that the reduction in size due to the scar shrinkage might be negligible. Microscopic observations of the HE-stained specimens indicate that the affected area exhibited nuclear shrinkage and loss of muscle striations (Fig. 4b) in comparison with the normal area (Fig. 4c). These tissue changes might induce a permanent electrical conduction block.

DISCUSSION

The estimated length of the shortest path to wrap around the irradiation line (Fig. 1) indicates that the change in the conduction pathway might be 22 mm. The conduction delay corresponding to the expected conduction pathway change is calculated to be 22–55 milliseconds with the reported conduction velocity in the mammalian atrial appendage of 0.4–1.0 m/second [26]. The measured conduction delay of 35.5 milliseconds is within the range of the above calculated value. These results suggest that the conduction delay is due to the change in the conduction pathway induced by transmural myocardial electrical conduction block obtained immediately after the photosensitization reaction. In the short drug–light interval condition, the photosensitizer might be distributed mainly in the blood and interstitial spaces of myocardium; it is reported that NPe6 might get into the interstitial spaces <20 minutes after the injection [27,28]. The photosensitization reaction with an interstitial space-distributed photosensitizer might induce immediate necrotic-like cell damage, which may be responsible for the acute myocardial electrical conduction block [25,29]. Our previous report indicates that the damage to ion channels and cell membranes induced by the photosensitization reaction might cause an influx of Ca^{2+}, rapid increase in the intracellular Ca^{2+} concentration, and eventually a necrotic cell response [29]. The acute myocardial electrical response to the photosensitization reaction

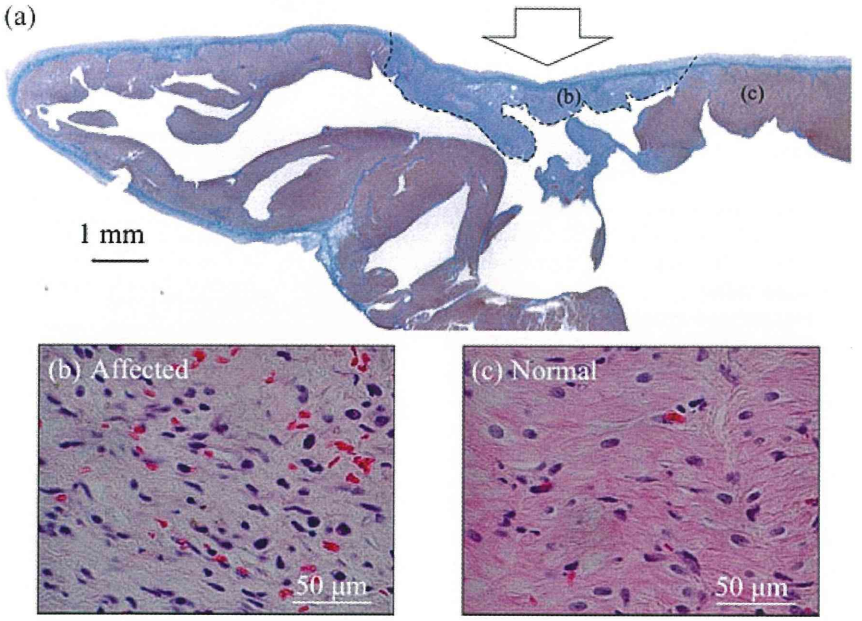

Fig. 4. **a**: An Azan-stained specimen of the irradiated area of a porcine left atrial appendage. The red laser light was irradiated from the direction of the arrow with a spot size of 3 mm, power density of 3.5 W/cm^2, and total energy density of 50 J/cm^2. The border between the affected and normal region was demarcated by the black dotted line. **b**,**c**: The HE-stained specimens of (b) the affected area and (c) the normal area indicated in (a).

was also demonstrated by the authors with exposed rat hearts *in vivo* [25].

The affected tissue depth by the photosensitization reaction obtained in the chronic histopathological study is reasonable on the basis of the measured optical penetration depth in the myocardium of 0.96 mm at 663 nm. As the condition of the photosensitization reaction is almost the same between the acute and chronic phase study, these results suggested that the acute electrical conduction block obtained in the electrophysiological evaluation might be kept in the chronic case. The observed tissue changes might be due to the oxidative process with the photosensitization reaction and not the thermal process, because the tissue temperature during the irradiation on the myocardial surface was <50°C for irradiation durations <30 seconds. It is reported that irreversible thermal damage in myocardium, including irreversible cellular electrophysiological changes and thermal denaturation is observed at temperatures exceeding 50°C for several minutes [30,31]. The temperature increase of the myocardium is rather small with the photosensitization reaction, compared to thermal ablation therapies in which the maximum temperature of the myocardial surface during the ablation is around 80°C [32,33]. The small temperature increase in the photosensitization reaction might be due to the low input power; the input power required to create a myocardial lesion with 2–3 mm in diameter and several millimeter deep may be <1 W for the photosensitization reaction, and is reported to be 10–30 W for laser ablation [7–9], and 20–50 W for radiofrequency ablation [32]. The energy consumption used for singlet oxygen generation in the photosensitization reaction with NPe6 is roughly estimated to be 1.9% of the total input energy under the experimental conditions, by considering (i) a molar absorption coefficient of NPe6, (ii) a quantum yield of singlet oxygen generation, and (iii) a NPe6 concentration in myocardium [18,21]. In contrast, almost all of the total input energy is used to generate heat in the thermal ablations. Therefore, the process of myocardial tissue damage with oxidative interaction in the photosensitization reaction is energy efficient. We think that catheterization application to cardiac ablation with the photosensitization reaction may be promising approach in non-thermal arrhythmia therapy, because temperature increase of the irradiated tissue might be suppressed by cooling effect of blood flow.

The electrophysiology and histology evaluation were conducted with healthy young pigs. Due to the rapid clearance of NPe6 from the body, large amount of the photosensitizer dose was needed in order to obtain optimal condition of photosensitizer concentration in plasma during the procedure, so that young light-weight pigs were used. In the case of human, the excretion rate of NPe6 is slower than that in animals; the elimination half-life of NPe6 is about 9 hours, so that the plasma concentration of the photosensitizer might be almost constant for several hours after the injection [17]. The myocardium of arrhythmia patients might have different structure and

function to the normal one; the optical properties and photosensitizer pharmacokinetics in the myocardium may change with the disease progression, such as collagen content of the myocardium. These factors need to be taken into account when determining the treatment protocol for clinical studies. In the measurement of the optical properties, we used ventricular tissue rather than atrial tissue. The measured optical properties of atrial ($n = 2$) and ventricular myocardium ($n = 16$) were almost the same, so that we showed the results with ventricular myocardium as the statistically collected value.

In conclusion, we demonstrated acute and chronic myocardial electrical conduction blocks as a result of the photosensitization reaction with NPe6 in the porcine left atrial appendage. The electrophysiological study indicated that the photosensitization reaction induced acute electrical conduction block according to the conduction delay of the electrical signal. The histopathological study showed that the photosensitization reaction induced transmural tissue scarring, indicating permanent electrical conduction block. These results indicate that a nonthermal catheter ablation using a photosensitization reaction could be applied in arrhythmia therapy.

ACKNOWLEDGMENTS

This study was partially supported by the Supporting Program for Creating University Ventures (#1904) of the Japan Science and Technology Agency and Research Fellowships of the Japan Society for the Promotion of Science for Young Scientists.

REFERENCES

1. Camm AJ, Kirchhof P, Lip GYH, Schotten U, Savelieva I, Ernst S, Van Gelder IC, Al-Attar N, Hindricks G, Prendergast B, Heidbuchel H, Alfieri O, Angelini A, Atar D, Colonna P, De Caterina R, De Sutter J, Goette A, Gorenek B, Heldal M, Hohloser SH, Kolh P, Heuzey JYL, Ponikowski P, Rutten FH. Guidelines for the management of atrial fibrillation. Eur Heart J 2010;31:2369–2429.
2. Nault I, Miyazaki S, Forclaz A, Wright M, Jadidi A, Jais P, Hocini M, Haissaguerre M. Drugs vs. ablation for the treatment of atrial fibrillation: The evidence supporting catheter ablation. Eur Heart J 2010;31:1046–1054.
3. Wazni OM, Marrouche NF, Martin DO, Verma A, Bhargava M, Saliba W, Bash D, Schweikert R, Brachmann J, Gunther J, Gutleben K, Pisano E, Potenza D, Fanelli R, Raviele A, Themistoclakis S, Rossillo A, Bonso A, Natale A. Radiofrequency ablation vs. antiarrhythmic drugs as first-line treatment of symptomatic atrial fibrillation. JAMA 2005;293: 2634–2640.
4. Cappato R, Calkins H, Chen SA, Davies W, Iesaka Y, Kalman J, Kim YH, Klein G, Natale A, Packer D, Skanes A, Ambrogi F, Biganzoli E. Updated worldwide survey on the methods, efficacy, and safety of catheter ablation for human atrial fibrillation. Circ Arrhythm Electrophysiol 2010;3:32–38.
5. Dagres N, Hindricks G, Kottkamp H, Sommer P, Gaspar T, Bode K, Arya A, Husser D, Rallidis LS, Kremastinos DTH, Piorkowski C. Complications of atrial fibrillation ablation in a high-volume center in 1,000 procedures: Still cause for concern. J Cardiovasc Electrophysiol 2009;20:1014–1019.
6. Cappato R, Calkins H, Chen SA, Davies W, Iesaka Y, Kalman J, Kim YH, Klein G, Packer D, Skanes A. Worldwide survey on the methods, efficacy, and safety of catheter ablation for human atrial fibrillation. Circulation 2005;111: 1100–1105.
7. Thomas SP, Guy DJR, Rees A, Collins L, Ross DL. Production of narrow but deep lesions suitable for ablation of atrial fibrillation using a saline-cooled narrow beam Nd:YAG laser catheter. Lasers Surg Med 2001;38:375–380.
8. Curtis AB, Mansour M, Fridel SE, Tomaru T, Barbeau GR, Normann SJ, Abela GS. Modification of atrioventricular conduction using a combined laser-electrode catheter. Pacing Clin Electrophysiol 1994;17:337–348.
9. Wagshall A, Abela GS, Maheshwari A, Gupta A, Bowden R, Huang SKS. A novel catheter design for laser photocoagulation of the myocardium to ablate ventricular tachycardia. J Interv Card Electrophysiol 2002;7:13–22.
10. Dougherty TJ, Gomer CJ, Henderson BW, Jori G, Kessel D, Korbelik M, Moan J, Peng Q. Photodynamic therapy. J Natl Cancer Inst 1998;90:889–905.
11. Schuitmaker JJ, Baas P, van Leengoed HL, van der Meulen FW, Star WM, van Zandwijk N. Photodynamic therapy: A promising new modality for the treatment of cancer. J Photochem Photobiol B 1996;34:3–12.
12. Dougherty TJ. Photodynamic therapy. Photochem Photobiol 1993;58:895–900.
13. Moore JV, West CML, Whitehurst C. The biology of photodynamic therapy. Phys Med Biol 1997;42:913–935.
14. Oleinick NL, Morris RL, Belichenko I. The role of apoptosis in response to photodynamic therapy: What, where, why, and how. Photochem Photobiol Sci 2002;1:1–21.
15. Buytaert E, Dewaele M, Agostinis P. Molecular effectors of multiple cell death pathways initiated by photodynamic therapy. Biochim Biophys Acta 2007;1776:86–107.
16. Kato H, Furukawa K, Sato M, Okunaka T, Kusunoki Y, Kawahara M, Fukuoka M, Miyazawa T, Yana T, Matsui K, Shiraishi T, Horinouchi H. Phase II clinical study of photodynamic therapy using mono-L-aspartyl chlorin e6 and diode laser for early superficial squamous cell carcinoma of the lung. Lung Cancer 2003;42:103–111.
17. Kessel D. Pharmacokinetics of N-aspartyl chlorin e6 in cancer patients. J Photochem Photobiol B 1997;39:81–83.
18. Spikes JD, Bommer JC. Photosensitizing properties of mono-L-aspartyl chlorin e6 (NPe6): A candidate sensitizer for the photodynamic therapy of tumors. J Photochem Photobiol B 1993;17:135–143.
19. Cheong WF, Prahl SA, Welch AJ. A review of the optical properties of biological tissues. IEEE J Quantum Electron 1990;26:2166–2185.
20. Star WM, Marijnissen JPA, van Gernert MJC. Light dosimetry in optical phantoms and in tissues: I. Multiple flux and transport theory. Phys Med Biol 1988;33:437–454.
21. Gomer CJ, Ferrario A. Tissue distribution and photosensitizing properties of mono-L-aspartyl chlorin e6 in a mouse tumor model. Cancer Res 1990;50:3985–3990.
22. Pickering JW, Bosman S, Posthumus P, Blokland P, Beek JF, van Gemert MJ. Changes in the optical properties (at 632.8nm) of slowly heated myocardium. Appl Opt 1993;32: 367–371.
23. Swartling J, Pålsson S, Platonov P, Olsson SB, Andersson-Engels S. Changes in tissue optical properties due to radiofrequency ablation of myocardium. Med Biol Eng Comput 2003;41:403–409.
24. Kondo K, Miyoshi T, Fujino H, Takizawa H, Imai S, Kobayashi N, Kenzaki K, Sakiyama S, Tangoku A. Photodynamic therapy using a second generation photosensitizer, Talaporfin. Photodiagnosis Photodyn Ther 2007;4:269–274.
25. Ito A, Hosokawa S, Miyoshi S, Soejima K, Ogawa S, Arai T. The myocardial electrical blockade induced by photosensitization reaction. IEEE Trans Biomed Eng 2010;57: 488–495.
26. Draper MH, Mya-TU M. A comparison of the conduction velocity in cardiac tissues of various mammals. Q J Exp Physiol Cogn Med Sci 1959;44:91–109.
27. Mitra S, Foster TH. In vivo confocal fluorescence imaging of the intratumor distribution of the photosensitizer mono-L-aspartylchlorin-e6. Neoplasia 2008;10:429–438.
28. Pegaz B, Debefve E, Borle F, Ballini JP, Wagnieres G, Spaniol S, Albrecht V, Scheglmann D, Nifantiev NE, van den Bergh H, Konan YN. Preclinical evaluation of a novel

water-soluble chlorin e6 derivative (BLC 1010) as photosensitizer for the closure of the neovessels. Photochem Photobiol 2005;81:1505–1510.
29. Ito A, Kimura T, Miyoshi S, Ogawa S, Arai T. Photosensitization reaction-induced acute electrophysiological cell response of rat myocardial cells in short loading periods of talaporfin sodium or porfimer sodium. Photochem Photobiol 2011;87:199–207.
30. Haines DE. The biophysics of radiofrequency catheter ablation in the heart: The importance of temperature monitoring. Pacing Clin Electrophysiol 1993;16:586–591.
31. Whayne JG, Nath S, Haines DE. Microwave catheter ablation of myocardium in vitro. Assessment of the characteristics of tissue heating and injury. Circulation 1994;89:2390–2395.
32. Wittkampf FH, Nakagawa H. RF catheter ablation: Lessons on lesions. Pacing Clin Electrophysiol 2006;29:1285–1297.
33. Matsudaira K, Nakagawa H, Wittkampf FH, Yamanashi WS, Imai S, Pitha JV, Lazzara R, Jackman WM. High incidence of thrombus formation without impedance rise during radiofrequency ablation using electrode temperature control. Pacing Clin Electrophysiol 2003;26:1227–1237.

J Artif Organs (2011) 14:171–177
DOI 10.1007/s10047-011-0578-4

MINIREVIEW

Tissue engineering and cell-based therapy toward integrated strategy with artificial organs

Satoshi Gojo · Masashi Toyoda · Akihiro Umezawa

Received: 9 May 2011 / Accepted: 19 May 2011 / Published online: 10 June 2011

Abstract Research in order that artificial organs can supplement or completely replace the functions of impaired or damaged tissues and internal organs has been underway for many years. The recent clinical development of implantable left ventricular assist devices has revolutionized the treatment of patients with heart failure. The emerging field of regenerative medicine, which uses human cells and tissues to regenerate internal organs, is now advancing from basic and clinical research to clinical application. In this review, we focus on the novel biomaterials, i.e., fusion protein, and approaches such as three-dimensional and whole-organ tissue engineering. We also compare induced pluripotent stem cells, directly reprogrammed cardiomyocytes, and somatic stem cells for cell source of future cell-based therapy. Integrated strategy of artificial organ and tissue engineering/regenerative medicine should give rise to a new era of medical treatment to organ failure.

This article is a translation of an article that appeared in *The Japanese Journal of Artificial Organs* 2010;39:202–207.

S. Gojo (✉)
Department of Therapeutic Strategy for Heart Failure,
Graduate School of Medicine, University of Tokyo,
7-3-1 Hongo, Bunkyo, Tokyo 113-8655, Japan
e-mail: satoshigojo-tky@umin.ac.jp

M. Toyoda
Research Team for Vascular Medicine,
Tokyo Metropolitan Institute of Gerontology, Tokyo, Japan

A. Umezawa (✉)
Department of Reproductive Biology,
National Institute for Child Health and Development,
2-10-1, Okura, Setagaya, Tokyo 157-8535, Japan
e-mail: umezawa@1985.jukuin.keio.ac.jp

Keywords Biofabrication · Stem cell · Reprogramming · Direct conversion · Clinical trial

Introduction

The human body is made up of approximately 60 trillion cells but can be traced back to one fertilized egg created by the union of an ovum and a sperm. The fertilized egg divides repeatedly, creating various cells that coordinate with each other to form all the different tissues and organs, ultimately leading to the formation of a complete individual. Whereas the human genome has been almost completely decoded and the genes involved in various mechanisms of the body are becoming known, many parts of this epic developmental process remain unclear. However, because these developmental mechanisms are closely related to the homeostatic maintenance and the regenerative mechanisms of organs and tissues, the field of regenerative medicine, which aims to use these mechanisms to treat diseases, is expanding rapidly.

Tissue engineering

Fusion protein

Biological tissue is composed not only of cells but also of a surrounding environment that is crucial in maintaining cell function in vivo and in homeostasis. Most importantly, the extracellular matrix is known to have dynamic and functional roles, such as providing a scaffold for cell adhesion (basement membrane and fibronectins) as well as maintaining and providing growth factors (heparan sulfate). Technological development with respect to manipulating

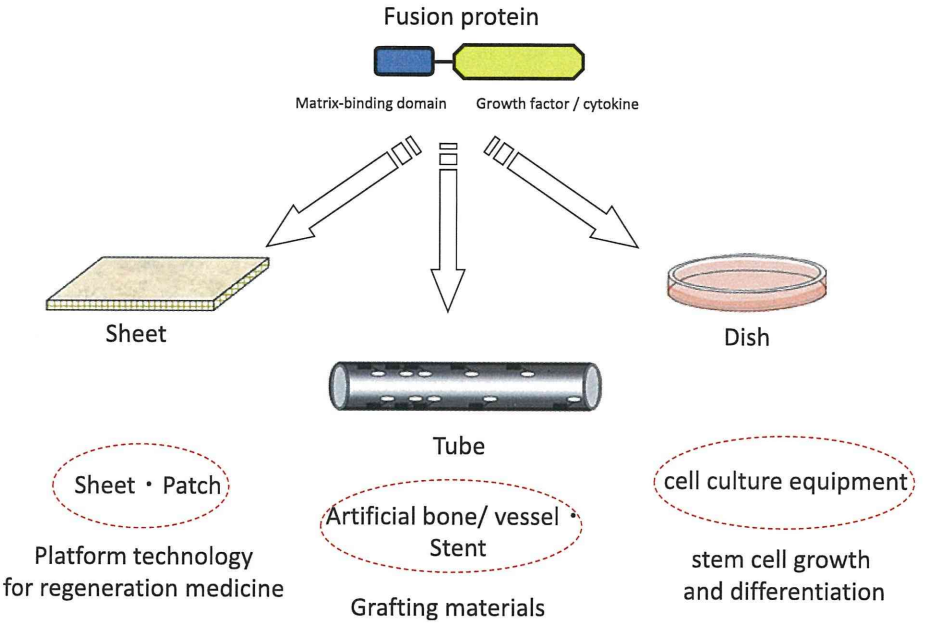

Fig. 1 Tissue engineering for regenerative medicine

this extracellular matrix in order to control tissues and cells, and its subsequent application in regenerative medicine, is underway. For example, studies have revealed that a variety of growth factors play important roles in wound healing, and some of these growth factors are in clinical use. However, the short-term effects of these growth factors pose some limitations on their use. An example is provided by fibrin, which is released in the wounded area when tissue damage occurs. An increasing amount of research is being conducted on the use of fibrin as a material for tissue regeneration. If a protein produced by the fusion of a fibrin-binding domain (FBD) to epidermal growth factor (EGF) is added to an epidermal wound-model culture system, binding of the growth factor to the fibrin released from the wound leads to healing by stimulating growth in the surrounding cells [1]. This phenomenon presumably occurs not because of the independent function of the growth factor, but because the growth factor stabilizes after binding to fibrin, and the FBD–EGF complex causes continuous cell stimulation. This suggests that the process of altering the combination of extracellular matrix and growth factors can be of therapeutic value in a variety of conditions. Another example can be considered with respect to vascular grafts. The development of small-caliber vascular grafts, such as those used to treat coronary artery disease, has slowed down because these grafts tend to fail at an early stage owing to thrombotic occlusion. To prevent this, prompt graft endothelialization and prevention of blood clot adherence is necessary. The use of a protein produced by fusion of the collagen-binding domain (CBD)—which binds collagen (a component of the extracellular matrix)—to hepatocyte growth factor (HGF) has been considered in such cases, and it has been shown that this complex (CBD–HGF) effectively promotes growth of endothelial cells [2]. Furthermore, this type of fusion protein could be placed onto a biodegradable sheet of extracellular matrix and affixed to the wounded area, where it may stimulate vascular cell growth. This has the potential for a wide application in medicine (Fig. 1).

Three-dimensional tissue engineering

A substantial amount of tissue engineering research has been performed on the three-piece that are cell, growth factors, and scaffolds. There are, however, various limitations to using scaffolds. First, cells tend to be distributed over the surface of the scaffold, thus making it difficult to form a solid tissue. Second, a 3D array and structure cannot be controlled when multiple cell types are used. Third, the concentration gradient of growth factors cannot be controlled. Fourth, there are certain limitations to the process of creating the vasa vasorum by tissue engineering techniques. In recent years, the concept of the scaffold has been put aside, and attempts to construct 3D tissue with cells and growth factors are now frequently reported. This method is generally called biofabrication [3], and the techniques of bioprinting [4] and organ printing [5] also fit into this category. In addition, although 3D structures using inkjet printer technology have already appeared as rapid prototyping, a 3D printer with an inkjet nozzle from which

droplets with a volume identical to that of cells are embossed, and which can be operated in a sterile environment, has been developed [6]. This could make the construction of 3D tissues possible [7]. Biorapid prototyping, a method in which many cellular spheres are used together with arbitrary structures to create 3D tissue, has also been reported [8]. This is expected to be an extremely promising methodology despite many issues, such as those related to cell solvents.

Cell sheets

Of all the recently developed tissue engineering techniques, practical application of cell sheets has advanced the most. This technology is based on the properties of a temperature-responsive polymer, poly(*N*-isopropylacrylamide). Culture dishes coated with this material are hydrophobic at 37°C and hydrophilic <32°C. When cells are cultured to confluence, they can be recovered as a sheet without enzymatic digestion [9]. This technique has been made available from Japan for worldwide application in the development of regenerative medicine-related products [10]. It was reported that stratification, which was initially limited to a few layers, could evolve to include many layers with neovascularization. So far, cell sheets have been made that consist of myoblasts [11], mesenchymal stem cells [12], cardiac progenitor cells [13], and a mixture of fibroblasts and endothelial progenitors [14]. Osaka University is coordinating a clinical trial using autologous myoblast sheets in patients carrying a left ventricular assist device (LVAD) with the aim of providing a bridge to recovery. In France, a clinical trial using epithelial cell sheets for corneal regeneration is being conducted by a venture company.

Whole-organ tissue engineering

The technology of perfusion decellularization of organs is a unique method of tissue production using scaffolds that has been reported in recent years. Intracellular structures can be completely eliminated by perfusing the heart using a Langendorff coronary perfusion apparatus for more than 12 h with the surfactant sodium dodecyl sulfate. It has also been reported that components of the extracellular matrix, including collagen type I/III, laminin, and fibronectin, can be preserved without disturbing their array structure; furthermore, the structure of valves and basal membrane of the epicardial vessels are not affected [15]. A heartbeat, albeit faint, has been achieved using this technique. The feasibility of whole-organ decellularization has been demonstrated in the pig heart [16] and rat liver [17]. Although the process of cellularization has its flaws, it is a creative initiative that holds promise for future developments.

Regenerative medicine

Induced pluripotent stem cells (iPSC)

The term regenerative medicine was introduced in 2000. Clinical applications have increased greatly since then, beginning with research on human embryonic stem cells (ESC) and confirmation of the plasticity of somatic stem cells. Amid frustration that human ESC could not be applicable not only to medicine, but also in biological research, the phenomenon of initialization via nuclear transplantation has been achieved in an elaborately planned experiment with four gene transfers. Now, these cells, called induced pluripotent stem cells (iPSC), certainly appear to be a major topic in regenerative medicine. Basic research into the clinical application of iPSC demonstrated the successful treatment of model mice for Parkinson's disease [18], sickle cell anemia [19], and hemophilia [20] with mouse iPSC. These reports indicate the same scheme could be applicable to human diseases. However, problems in iPSC application include the development of teratomas from undifferentiated cells, carcinomas due to gene transfer, and infection with xenogeneic materials used in cell cultures. These problems have attracted the interest of a large number of researchers, and many proposals for solutions to them have been reported (Fig. 2).

Teratoma formation in mice can reportedly be prevented by eliminating stage-specific embryonic antigen-1-positive cells [18]. If the target of interest is the heart, enrichment with mitochondria could prevent teratoma formation [21]. Of the four genes transferred during iPSC initialization, which are considered to be reprogramming genes, it was feared that the existence of c-Myc, in particular, which is an oncogene, would lead to cancer; carcinogenesis through c-Myc reactivation was actually observed in vivo. In addition, because the basic protocol uses a retrovirus as the vector for gene transfer, the possibility of carcinogenesis after its insertion into a genome is a problem. It was subsequently reported that just three factors (excluding c-Myc) induced iPSC, albeit at a low frequency [22]. However, recently, induction of iPSC with RNA [23] and proteins [24] of reprogramming factors has been reported in an attempt to circumvent carcinogenesis because of the methodology. Of the four factors, Sox2 and c-Myc could be replaced with transforming growth factor-α receptor antagonists [25], the nuclear acceptor Esrrb could be replaced with Klf4 [26], and Oct4 could be replaced with nuclear acceptor Nr5a2 [27].

Currently, xenogeneic materials are used in various processes in standard ESC/iPSC culture (Fig. 3). Feeder cells are used to maintain the undifferentiated state of both ESC and iPSC; usually, mouse embryonic fibroblasts (MEF) treated with mitomycin C to arrest their growth are

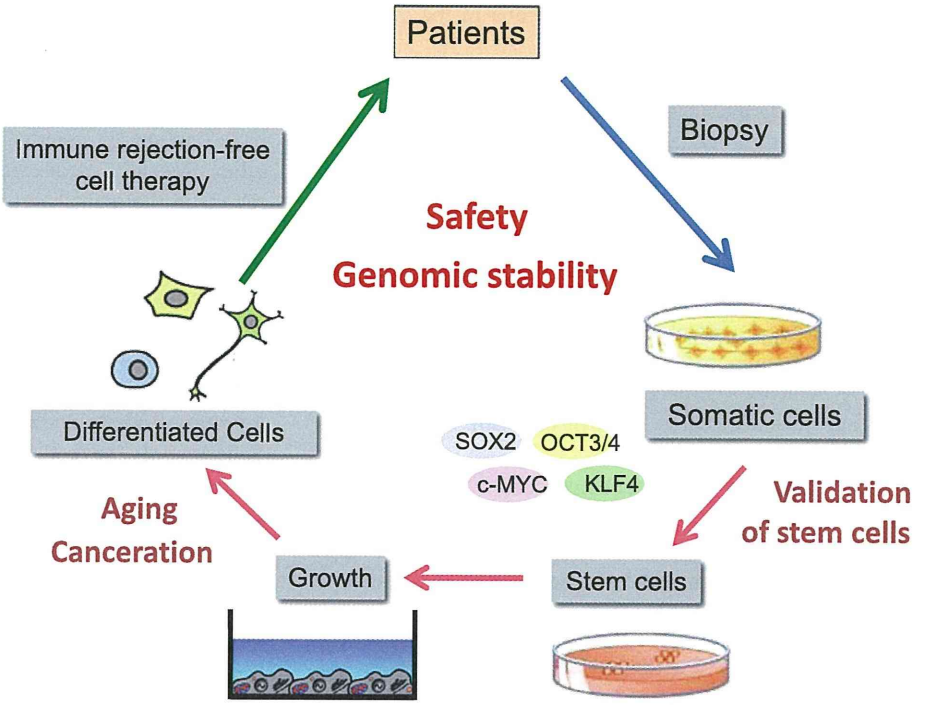

Fig. 2 Order-made stem cell therapy

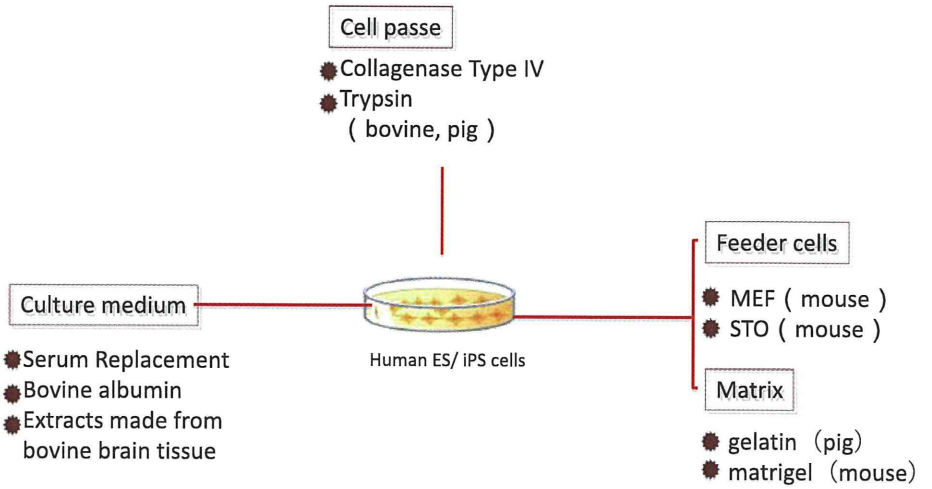

Fig. 3 Xenogeneic factors and materials in human embryonic stem cell/induced pluripotent stem cell (ESC/iPSC) culture

used as feeder cells. It was feared that if these xenogeneic cells were used in clinical situations, contamination with xenogeneic cells may lead to infection. This did, in fact, occur: the presence of non-human-derived Neu5Gc was confirmed on the cell surface of human ESC cultured onto MEF. Many individuals possess antibodies for this antigen, and an immune reaction can be provoked in these individuals [28]. In order to avoid xenogeneic contamination, coating cell culture dishes with fully synthetic compounds and the chemical defined-culture medium has been reported from several institutes. A 3D porous natural polymer scaffold consisting of chitosan and alginate was able to sustain human ESC self-renewal [29]. Recombinant vitronectin also supported cultivation of three human ESC under feeder-free conditions [30]. Moreover, suspension culture of human ESC and iPSC in chemically defined media supplied a scalable number of cells [31]. However, the ability of xeno-free protocols to maintain the self-renewal ability and pluripotency of human ESC or iPSC remains questionable. On the other hand, autologous